UNIVERSITY OF CALIFORNIA, SAN DIEGO

Buoyancy-based separation of antigen-specific T cells

A dissertation submitted in partial satisfaction of the requirements for the degree
Doctor of Philosophy

in

Bioengineering

by

Xiaoyu Shi

Committee in charge:

Professor Klaus Ley, Chair
Professor Shankar Subramaniam, Co-chair
Professor Pedro Cabrales
Professor Juan Carlos del Alamo
Professor Joshua Rychak
Professor John Watson

2016

The Dissertation of Xiaoyu Shi is approved, and it is acceptable in quality and form for publication on microfilm and electronically:

_____

_____

_____

_____

_____

Co-Chair

_____

Chair

University of California, San Diego

2016

DEDICATION

To the two rental cars I lived out of during part of grad school:

Pathfinder (ALM6444) and *Rover 02* (7SUG953), farewell, and thank you.

For the mice.

TABLE OF CONTENTS

LIST OF FIGURES

LIST OF TABLES

LIST OF ABBREVIATIONS

Ab/α	Antibody
ABS	Acrylonitrile butadiene styrene
APC	Antigen presenting cell/Allophycocyanin
ApoE	Apolipoprotein E
bCD4	biotinylated antibody directed against CD4
CAD	Computer-aided design
CDx	Cluster of differentiation [x]
FACS	Fluorescence-activated cell sorting
FEA	Finite element analysis
FMO	Fluorescence-minus-one
HSC	Hematopoietic stem cell
MB	Microbubble
MHCII	Major histocompatibility complex class II
NMR	Nuclear magnetic resonance
RCSB PDB	Research Collaboratory for Structural Bioinformatics Protein Data Bank

PE	Phycoerythrin
PEG	Polyethylene glycol
SA	Streptavidin
TCR	T cell receptor

ACKNOWLEDGEMENTS

Dr. Klaus Ley (La Jolla Institute for Allergy and Immunology, La Jolla, CA; University of California San Diego, La Jolla, CA) served as committee chair for this project.

The Introduction, Results, and Discussion sections do not include published work, work submitted for publication, or material being prepared for publication submission. These sections include results generated as a result of collaboration with Dr. Joshua Rychak (Targeson, La Jolla, CA; University of California San Diego, La Jolla, CA), who provided microbubble reagents, Dr. Marc Jenkins (University of Minnesota, Minneapolis, MN), who provided biotinylated MHCII monomer, and Dr. Zbigniew Mikulski (La Jolla Institute for Allergy and Immunology, La Jolla, CA), who assisted with confocal microscopy. The dissertation author was the principal researcher and author on this dissertation.

This work was supported by NIH Grant Number 5 F31 EB019307-02 and PHS Grant Number 5 T32 HL 105373-3.

VITA

2010	Bachelor of Science in Engineering, University of Michigan
2013	Master of Science, University of California, San Diego
2016	Doctor of Philosophy, University of California, San Diego

ABSTRACT OF THE DISSERTATION

Buoyancy-Based Separation of Antigen-Specific T Cells

by

Xiaoyu Shi

Doctor of Philosophy in Bioengineering

University of California, San Diego, 2016

Professor Klaus Ley, Chair
Professor Shankar Subramaniam, Co-Chair

This project focuses on the proof-of-concept development of a separation construct to isolate antigen-specific CD4 T cells using a buoyant lipid microparticle (microbubble) reagent attaching major histocompatibility complex class II (MHCII) molecules. These cells are implicated in the progression of cardiovascular disease. The project relied critically on preexisting reagents produced by collaborators: microbubbles and biotinylated recombinant MHCII monomers.

Current cell separation methods rely primarily on either magnetic separation or flow-cytometry based sorting. The method presented here provides the basis for a new avenue of investigation using a principally different separation scheme based on buoyancy. It is intended to be extensible to the separation of antigen-specific T cells in other contexts and was originally intended to be a removable separation reagent (unsuccessful). The ultimate goal is the development of a separation system which may be used to further clinical work or research relying on cell isolation.

Here, the buoyancy-based method is first used to perform bulk B and CD4 T cell separations. These are common lab procedures for which many commercial kits are available, which made them an ideal testbed for initial study. Flow cytometric analysis and confocal microscopy were performed to confirm successful cell enrichment.

The separation system was then further developed to separate antigen-specific CD4 T cells reactive to the endogenous murine peptide P6 (TGAYSNASSTESASY), relevant in the study of atherosclerosis. Flow cytometric and microscopic confirmation of successful separation was performed in this section as well.

Several devices for centrifugation were designed and constructed in the course of this project. These attempted to create a pendant droplet between the buoyant and non-buoyant fractions in a single column of liquid formed by centrifugation, allowing for these layers to be completely sequestered from one another. Though these devices were unsuccessful, they merit further study. Another device, a centrifuge adapter, was created as an all-purpose experimental aid to hold and centrifuge all combinations of reagent tubes used in the cell separation protocol. Computer graphics animations and diagrams of

various facets of the project were also made, including molecular-scale models of separation constructs derived from Protein Data Bank (PDB) structural data.

INTRODUCTION

Modern immunology experiments and clinical procedures often require purified cell populations. In preclinical research, they can be inputs, providing homogeneous starting material for culturing, transplantation, or other studies that rely on consistency to generate meaningful results. In other settings, the purified cells themselves are the end goal. For example, purified hematopoietic stem cells (HSCs) have been used in bone marrow transplantation [1] and cytotoxic T cells in cancer treatment [2]. Another application is in-depth study of the phenotypes of purified T cell populations through proteomics and transcriptomics analysis [3], among other techniques. Further, vaccine efficacy could be monitored by examining antigen-specific T cells induced by vaccinations such as those for vaccinia virus [4].

Immune cell types

This work focuses on separation of immune cells, which can be broadly divided into two categories: adaptive and innate. Each category contains a very large and rich diversity of cell types, the precise delineation of which is beyond the scope and interest of the project. All immune cells ultimately originate from HSCs in the bone marrow.

Some of these precursor cells destined for the adaptive lineage journey to another primary lymphoid organ, the thymus, where they become T lymphocytes, whereas B lymphocytes complete their maturation in the bone marrow. T (signifying thymus) and B (first derived from the initialism of an organ in birds producing these cells, instead

produced in the bone marrow in humans and mice) cells comprise the majority of adaptive immune cells. Lymphocytes can be found not only in the blood, but also lymphatic fluid and secondary lymphoid organs, including lymph nodes. T lymphocytes, the separation of a subset of which is the main focus of this project, furthermore may be subdivided into many different types. Broadly, a given T lymphocyte expresses either the αβ or γδ heterodimeric form of the T cell receptor (TCR); furthermore, a mature αβ T lymphocyte is signified by the presence of one of two surface markers known as CD4 and CD8, using CD (cluster of differentiation) nomenclature. B lymphocytes progress through several stages of maturation, some of which can be characterized by the presence of the CD19 and CD45R (B220) cell surface molecules. The endpoint of B lymphocyte maturation is the transformation into a plasma cell, which is responsible for the generation of antibodies.

As for innate immune cells, broad categories include granulocytes, monocytes, dendritic cells. Granulocytes, which includes neutrophils, can be further subdivided into additional subtypes, some of which acquired their names from the incorporation of dyes such as hematoxylin and eosin and the resulting characteristic appearance (i.e., eosinophils). Innate immune cells are not the subject of this project, but they play critical roles in immune function.

The categories described above comprise the majority of immune cell types present in mice and humans.

Table 1. Cell types discussed in this work. This table presents the categorization of innate and adaptive immune cells for the purposes of this project by the presence of characteristic molecular cell surface markers. The fluorophore associated to each marker is refers to an antibody used to stain the marker for flow cytometric analysis of B cells, described later.

Marker	CD3e	CD8a	CD4	Ly-6C	Ly-6G	B220
Fluorophore	PE	FITC	PerCP	Pac. Blue	Pac. Org	AF647
Cell	T	CD8	CD4	Mono.	Neut.	B

Cell separation

Cell separation encounters three fundamental difficulties. First, cells are small. A representative lymphocyte from the mouse or human is approximately ten microns in diameter, making it impossible to see without microscopic aid. They are also mostly transparent, and many require staining with exogenous dyes or fluorescent antibodies to identify. T and B lymphocytes appear identical in light microscopy, yet have vast functional differences. Second, unwanted cells usually outnumber target cells, sometimes by orders of magnitude. For example, a researcher interested in separating CD4 T cells from a wild-type C57BL/6 spleen would find that the target population comprises less than 15 percent of the total number of splenocytes [5]. The antigen-specific cells described in this work further comprise less than 10 percent of the CD4 T cell population (of pooled lymph nodes). According to the laboratory of Marc Jenkins, antigen-specific CD4 T cells may number as few as 20 per mouse [6]. Third, cells are living. Subjecting them to harsh treatment compromises viability and function.

In summary, cells cannot be readily seen or manipulated without effort, and they are often located in complex, heterogeneous mixtures. Cell separation must contend with the added condition that the cells should be kept in their native state as much as possible.

This project focuses on immune cells. Current immunological cell separation is primarily accomplished through bulk sorting or by fluorescence-activated cell sorting (FACS).

Bulk sorting strategies include density gradient centrifugation and magnetic bead-based separation. In density gradient centrifugation, cells are layered on top of media

(Ficoll, a commercially-available polysaccharide [7,8], or Percoll, commercially-available coated silica particles [9], both used in media preparation for this technique), and then centrifuged. Cells separate according to their densities. This method can separate certain cells, such as erythrocytes, granulocytes, and mononuclear cells, but it cannot distinguish cells with the same density. For example, T and B lymphocytes cannot be resolved using this method.

In magnetic bead separation, antibodies against cell surface receptors are linked to metal beads, typically iron oxide nano- or microparticles. Commercially available kits for magnetic cell separation are produced by several manufacturers, such as Miltenyi, eBioscience, BioLegend, ThermoFisher, StemCell, and Becton Dickinson. Detailed product specifications from each manufacturer were proprietary. Table 2 lists available data from product data pages [10, 11, 12, 13, 14, 15]. Nanoparticles are commonly described as polydispersed, irregularly-shaped entities; microparticles are much larger (micron-sized) and more uniformly spherical. The antibodies linked to these metal particles target either receptors on the cell population of interest (positive selection), or may be a mix of antibodies targeting receptors not on the cells of interest (negative selection). Following attachment of the beads, the captured cell population is magnetically separated from unlabeled cells using a magnet. Some nanoparticle separation systems, such as those from Miltenyi, require separation using macro-sized magnetic particles or steel wool packed into a column, which are needed to potentiate the magnetic force used to capture the labeled cells [16, 17, 18].

Table 2. Enumeration of commercially available cell separation kits. Data collected from manufacturer product pages [10, 11, 12, 13, 14, 15].

Manufacturer	**Product**	**Particle scale**	**Uniformity**	**Protocol**
Miltenyi	MACS MicroBeads	Nanoparticle (50 nm)	Undisclosed	Column
eBioscience	MagniSort	Undisclosed; invisible to light microscopy, likely nanoparticle	Undisclosed	Column-free magnet
BioLegend	MojoSort	Nanoparticle (130 nm)	Undisclosed; likely polydispersed	Column-free magnet
ThermoFisher	Dynabeads	Micron	Monodispersed	Column-free magnet
StemCell Technologies	EasySep	Undisclosed; likely nanoparticle	Undisclosed	Column-free magnet
Becton Dickinson	IMag	Nanoparticle	Undisclosed; likely polydispersed	Column-free magnet

In FACS, cells are separated one at a time using a complicated instrument. Cells are labeled with antibodies as in the magnetic separation scheme, but the antibodies are attached to fluorescent molecules instead of magnetic beads. The fluorescence is detected with a laser as the cell passes through a fluidic system. The cell flow is set up such that cells are in a single-file arrangement by hydrodynamic focusing as they approach the analysis and sorting components. Fluorescently-labeled or unlabeled cells are then partitioned into droplets, which are then guided into different containers. One type of FACS system imparts electrical charge to droplets, which are deflected into the target container. Sorting via FACS results in the highest possible purity for cell separation, but the equipment is highly specialized and requires extensive infrastructure and expertise to operate. A modern FACS sorter such as the FACSAria can sort up to 50 million cells per hour, whereas a typical murine splenocyte preparation may contain 10^8 cells, making the method low-throughput in comparison to bulk sorting [18]. Additionally, sorting can be stressful for cells [19, 20, 21].

Ideally, cell separation proceeds with minimal interference to the cell's natural state. For example, cell separation of neutrophils typically follows a negative selection scheme because the separation procedure itself causes unwanted changes in the cell state [22]. However, in rare cell separation, it is impossible to avoid using positive selection. For example, this work describes a positive selection method to separate antigen-specific T cells. It is impossible to generate reagents to all possible unwanted entities to be negatively selected, as will be described shortly.

New reagents used

In this project, microbubbles are used to separate cells. The microbubbles were produced and prepared by a local company, Targeson, Inc. (La Jolla, CA), and were developed from ultrasound contrast agents. These are lipid microparticles filled with a gas such as perfluorobutane (C_4F_{10}), with a right-skewed size distribution ranging from sub-micron to over 10 microns in diameter, with one major lipid constituent being distearoylphosphatidylcholine (DSPC) [23, 24, 25]. The modal diameter is approximately 1.677 microns.

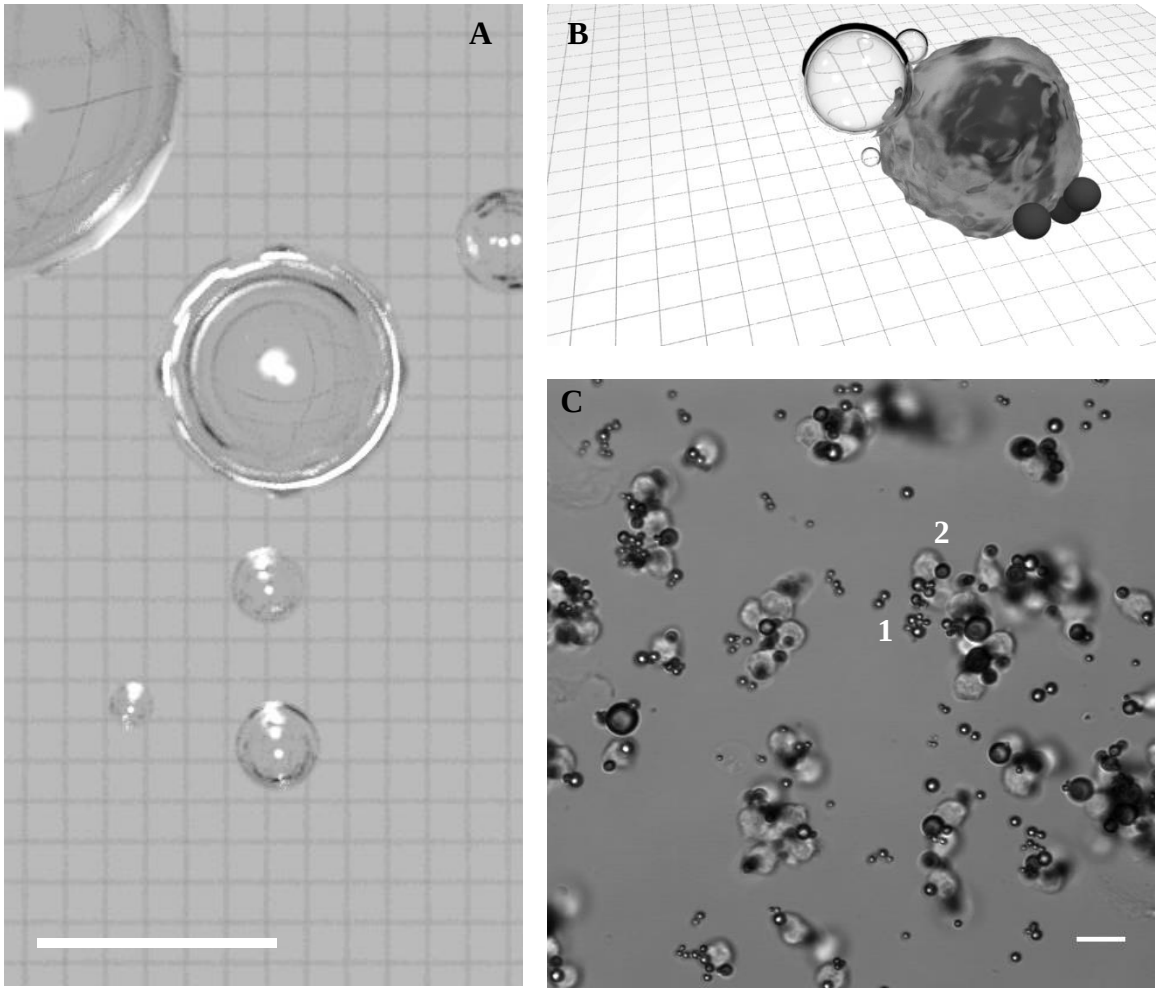

Figure 1. Microbubble visual appearance. (left) Computer simulated, raytraced appearance of microbubbles at $1{:}10^4$ scale (bar represents approximately 1.5 microns at this scale). Raytracing is a rendering method which involves calculating the interaction of virtual rays of light with the objects and associated materials they encounter as they traverse a virtual environment. Here it is used to demonstrate the characteristic refraction seen when viewing microbubbles in light microscopy. Note the distortion of the background grid lines. Gas volume of all bubbles was set at 99.5% of total volume. Refractive indices of gas and buffer approximated as air (n = 1) and water (n = 1.333). Created using Autodesk (San Rafael, CA) Maya modeling software using the NVIDIA (Santa Clara, CA) mental ray renderer. (top right) Computer render of polydispersed microbubbles, top left, and monodispersed iron oxide microparticles, bottom right, both attached to a leukocyte. The leukocyte model's outer surface is a modified mesh derived from a 3D neutrophil model reconstructed from the Leica (Wetzlar, Germany) SP5 confocal microscope, provided by Dr. Zbigniew Mikulski. (bottom right) Confocal micrograph of microbubbles (1), adjacent to cells (2). Scale bar is 10 microns. Microbubbles appear characteristically different in flow cytometry light scatter as well.

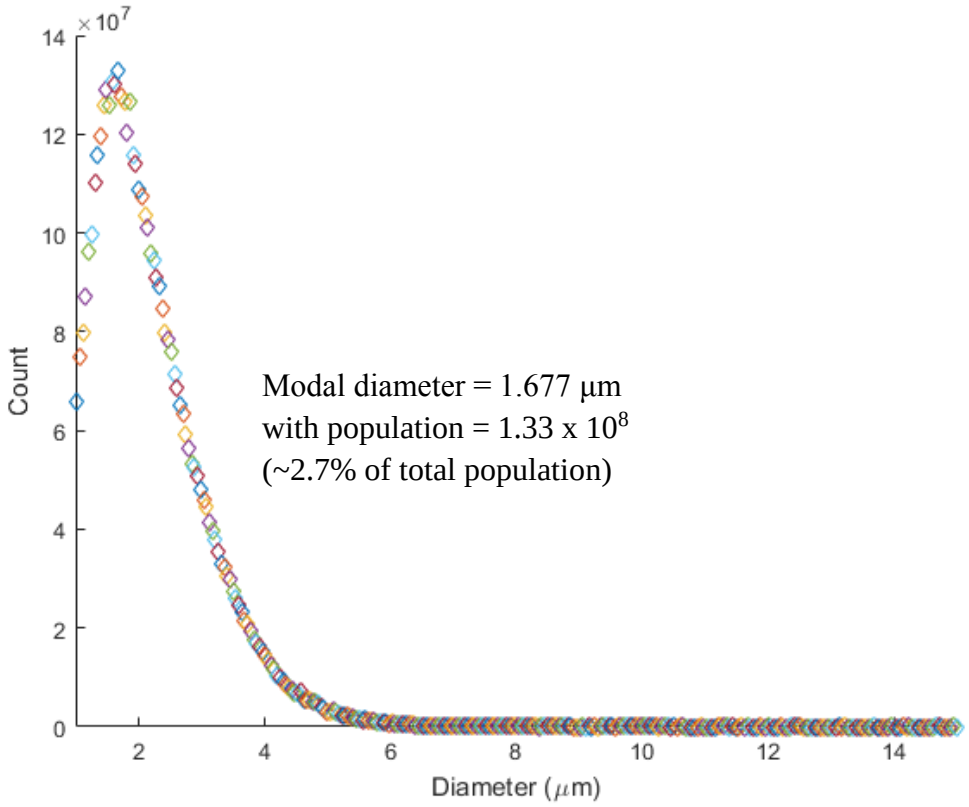

Figure 2. Exemplary size distribution of microbubbles. Adapted from CD19 microbubble size distribution data generated by Targeson.

The project's cell separation method relies on the buoyancy of the microbubble. On the surface of the microbubbles, antibodies against cell surface receptors were covalently attached. In other experiments, I used microbubbles coupled to streptavidin, a molecule with high affinity for biotin [26]. This microbubble can be labeled with any biotinylated species such as antibodies or MHCII monomers that would attach to the target cell of interest. Thus, there were two primary bubbles used in this work: a CD19 microbubble, in which anti-CD19 antibody was attached, and the streptavidin microbubble, in which streptavidin was attached. For the purposes of this project, a cell expressing CD19 was considered a B lymphocyte. As shown in Figure 1, microbubbles cause significant refraction of light when viewed under microscopy and visualized in a flow cytometry light scatter plot.

CD4 T cells recognize antigenic peptides which have been bound in the groove of MHCII molecules, as exemplified in Figure 3. Here, I used biotinylated recombinant MHCII with the specific peptide of interest covalently linked in the peptide binding groove. The mouse MHCII molecule I-A^b was modified, linked to peptide, and expressed as described by the Marc Jenkins laboratory in Minnesota [27]. These biotinylated I-A^b molecules were used in conjunction with the streptavidin microbubble, and in separate experiments were bound to streptavidin only to make MHC tetramers, or to a modified dextran molecule by Immudex (Copenhagen, Denmark) to make MHC dextramers. An early incarnation of one such scheme is shown in Figure 4. The reason for multimerization is due to the low affinity of single MHCII-TCR interaction [28]. Stable attachment required multiple weak interactions, as reminiscent of Velcro.

The Introduction, Results, and Discussion sections do not include published work, work submitted for publication, or material being prepared for publication submission. These sections include results generated as a result of collaboration with Dr. Joshua Rychak (Targeson, La Jolla, CA; University of California San Diego, La Jolla, CA), who provided microbubble reagents, Dr. Marc Jenkins (University of Minnesota, Minneapolis, MN), who provided biotinylated MHCII monomer, and Dr. Zbigniew Mikulski (La Jolla Institute for Allergy and Immunology, La Jolla, CA), who assisted with confocal microscopy. The dissertation author was the principal researcher and author on this dissertation.

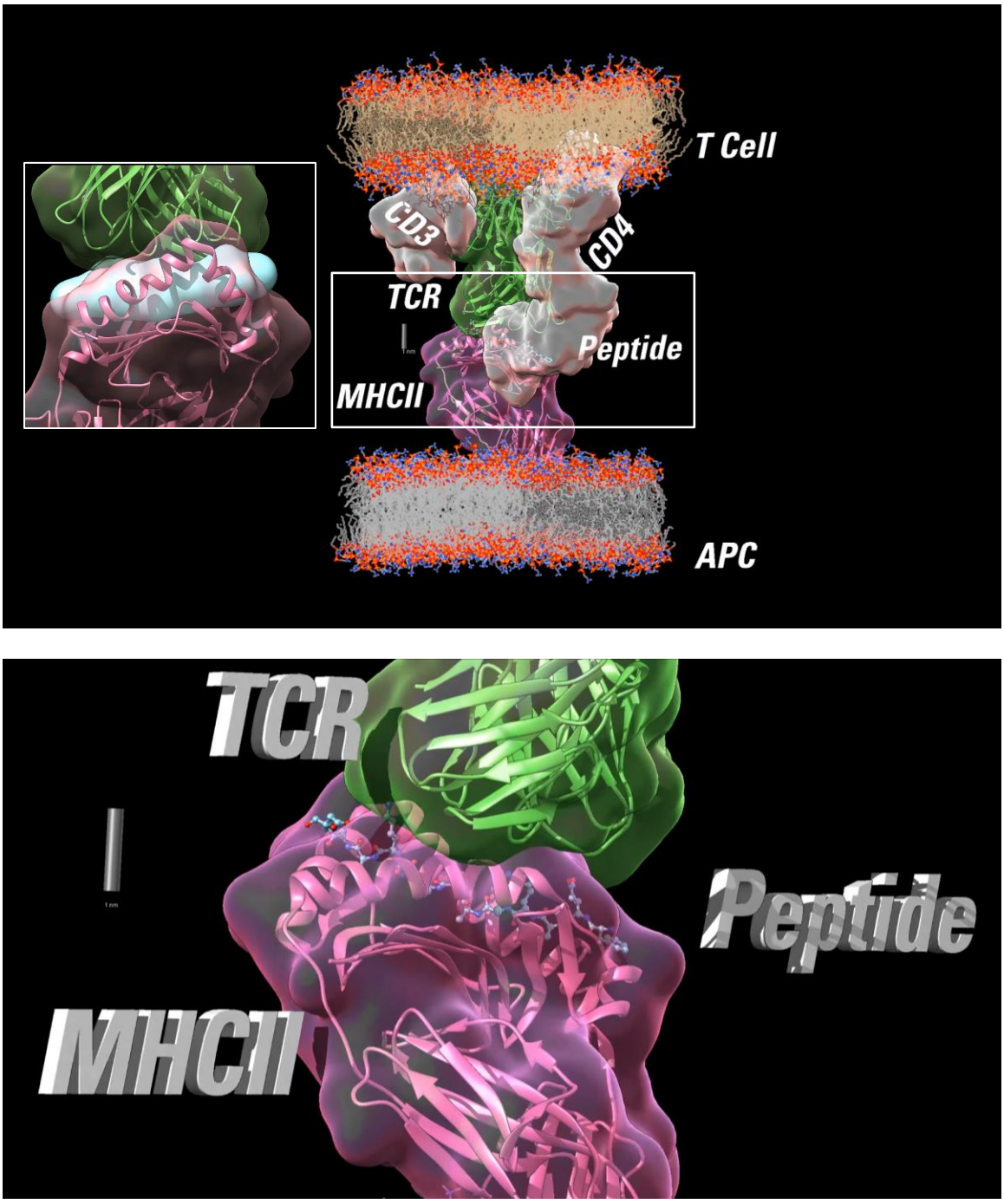

Figure 3. Antigen presentation to a CD4 T lymphocyte. Membrane bilayers for the T cell and antigen presenting cell (APC) are shown, with associated CD3 and CD4 surface molecules. A peptide 13 residues long resides is shown in the binding groove of the MHCII molecule. Gray scale bar is 1 nm. Molecular positions are approximated. Visualization created using UCSF Chimera software.

The previous figure was created using UCSF Chimera using modified structural data from RSCB PDB.

--UCSF Chimera--

"Molecular graphics and analyses were performed with the UCSF Chimera package. Chimera is developed by the Resource for Biocomputing, Visualization, and Informatics at the University of California, San Francisco (supported by NIGMS P41-GM103311)."

UCSF Chimera--a visualization system for exploratory research and analysis. Pettersen EF, Goddard TD, Huang CC, Couch GS, Greenblatt DM, Meng EC, Ferrin TE. J Comput Chem. 2004 Oct;25(13):1605-12.

--PDB--

PDB ID: 4P23
DOI: 10.4049/jimmunol.1303209

PDB ID: 2MLR
DOI: 10.1038/ncomms6552

PDB ID: 1WIP
DOI: 10.2210/pdb1wip/pdb

PDB ID: 2MIM
DOI: 10.2210/pdb2mim/pdb

www.rscb.org

H.M. Berman, J. Westbrook, Z. Feng, G. Gilliland, T.N. Bhat, H. Weissig, I.N. Shindyalov, P.E. Bourne (2000) The Protein Data Bank
Nucleic Acids Research, 28: 235-242.

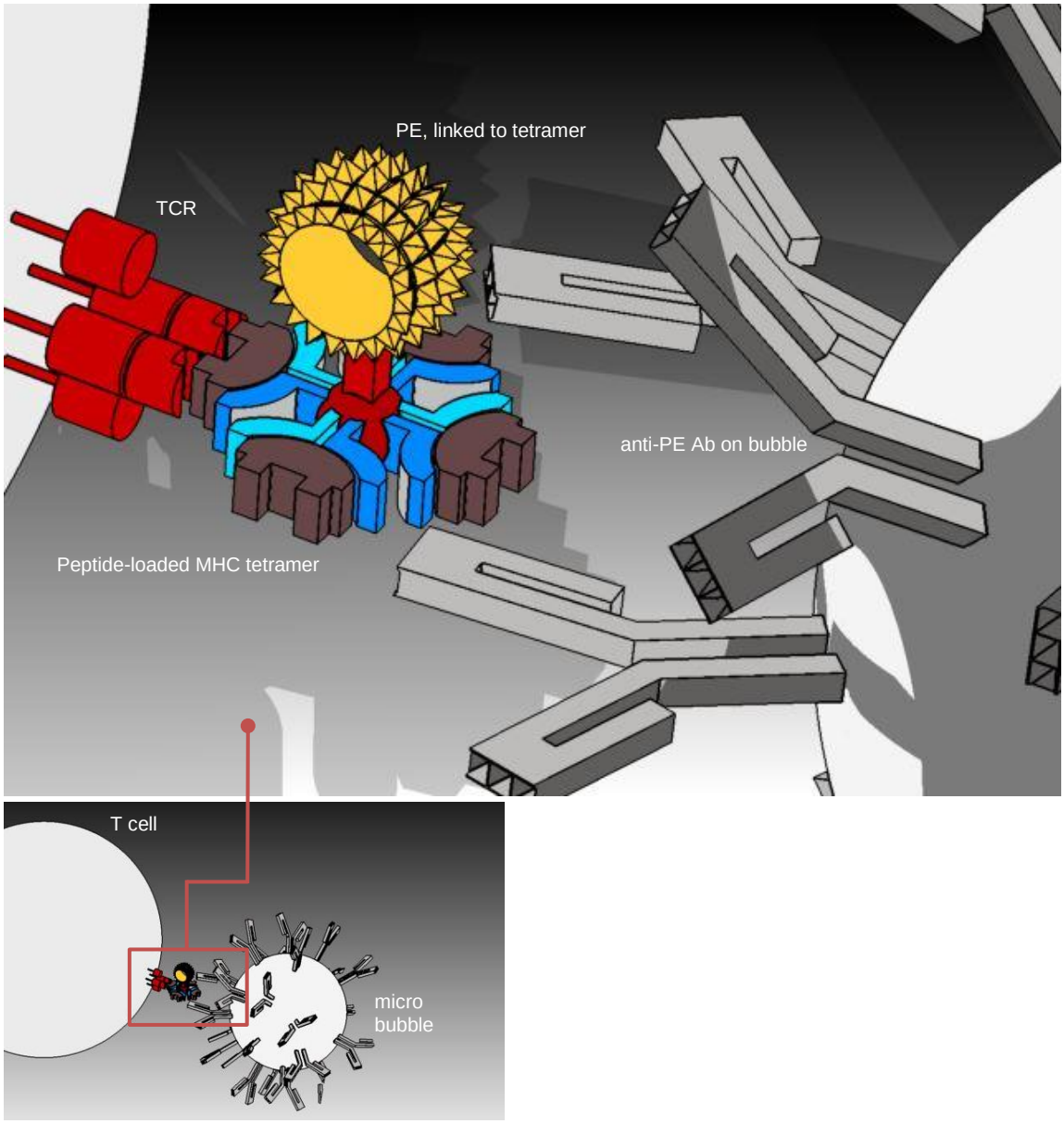

Figure 4. Example of MHCII microbubble construct. Streptavidin is shown in red in the center of the tetramer assembly. The two blue shaded entities represent α and β chains of the I-A^b molecules; brown represents the bound peptide. The clustered red molecules on the cell represent the T cell receptor on the target cell. The microbubble to the right is attached to antibodies against phycoerythrin (PE), a fluorophore, attached to the MHCII tetramer. This specific scheme was later superseded in favor of a streptavidin microbubble attaching biotinylated I-A^b molecules directly.

RESULTS

The ultimate goal of the work was to achieve separation of antigen-specific T cells using microbubbles and the biotinylated MHCII monomers. To do this, several preliminary experiments needed to be performed to set up the testing space and to confirm and quantify successful separation. B cell separations were initially performed before switching to CD4 T cell separation and finally antigen-specific T cell separation.

Cell culturing

Antigen-specific CD4 T lymphocytes were grown in culture to provide material for experiments. These cells were intended to be used as an abundant source of positive controls to test the separation method before looking for the corresponding cells *in vivo*, where the abundance would be far lower. Cells were harvested from peptide-vaccinated C57BL/6 mice [29], performed by Dr. Kevin Tse (La Jolla Institute for Allergy and Immunology, La Jolla, CA) or sent for culture by Dr. Harley Tse (Wayne State University, Detroit, MI). These cells were cultured in well plates and subsequently T-flasks coated with anti-CD3/CD28 antibody or co-incubated with irradiated splenocytes, two common strategies to induce T cell proliferation, using a protocol adapted from Dr. Harley Tse using RPMI media supplemented with fetal bovine serum, penicillin/streptomycin, HEPES, non-essential amino acids, sodium pyruvate, beta-mercaptoethanol, and glutamine [30, 31, 32]. These cells did not proliferate prodigiously despite several attempts, and attention was directed elsewhere.

Cell counting

An important aspect of the project is the need to determine statistics such as purity, viability, and yield with accuracy. To do this, accurate cell counting is crucial.

A commonly used method to count cells is the hemocytometer. Despite "-meter" in the name, this is a completely manual method to determine cell counts that involves pipetting a known volume, typically 10-20 uL, into a specially etched slide (Neubauer chamber, 100 micron depth, 1 mm^2 area) that is placed on a light microscope for viewing. The etch marks in the slide are arranged in a grid; the number of cells that fall within certain areas of the grid are counted and multiplied against a dilution factor. This gives the cell concentration. However, because this method is completely manual, it is subject to human error: improper dilution (either too few cells counted or too many cells that obscure the ability to keep track of cells already counted), inconsistency or not abiding by a convention in counting strategy (particularly with regard to cells that touch borders of the grid). Error is also inherent to the in low number of cells sampled for the count (typically 100). ASTM F2149, a cell counting standard, lists the error inherent to hemocytometry as between 10-30% [33]. When looking for rare cell populations whose prevalence could be as low as 2% of parent populations, this makes manual counting impossible.

Another common method to count cells is an extension of the hemocytometer, but incorporates the use of a camera and image recognition program to recognize and count cells. This method attempts to remove the operator bias by using a computer to classify what entities are cells. One such instrument is the ViCell (Beckman Coulter, Carlsbad,

CA) [34]. As with the hemocytometer, a known volume of sample to be counted is placed in a cuvette, which is then aspirated into the instrument, diluted further with a known volume of trypan blue to assess viability, and then flowed into an imaging chamber where pictures are acquired and then analyzed by the computer. Prior to counting, the operator must calibrate the image recognition program to instruct what image sections should be considered cells. This may include parameters such as brightness, general shape, and brightness of the center being examined. While an improvement over a hemocytometer because of the removal of bias of cell classification, this method still has its drawbacks. The computer will stringently apply the classification criteria, but the incarnation of the instrument that was available for such purpose for this project was unable to judge the appropriateness of the dilution factor. The range needed to obtain cell counts often required testing several samples at varying dilutions, resulting in much wasted sample. Further, very dilute samples count not be counted at all or required concentration by centrifugation, further introducing loss and variability into the method. Finally, the instrument took low-resolution images. Upon review, some images were mis-classified. Though the computer theoretically is the ultimate standard in consistency, these errors did not inspire confidence and a superior method was selected instead of attempting to further analyze the nature of the errors.

The superior method is electrozoning, or Coulter counting. This is a completely automated method in which a single cell suspension passes into a fluidic system that analyzes the change in electrical resistance as entities pass through a sensor in the instrument. Based on the resistance signal, the size of the object can be inferred accurately. Electrozoning is the method for which the ASTM F2149 engineering standard

exists. There are many such instruments, including the Beckman Coulter Multisizer (Beckman Coulter, Carlsbad, CA), and the Drew Scientific Hemavet (Drew Scientific, Miami Lakes, FL). The Multisizer can provide size distributions, which make it amenable for counting other entities, such as microbubbles, in addition to cells. Because of the nature of the counting method, electrozoning is insensitive to optical artifacts such as refractive index mismatches.

The Hemavet is a veterinary-grade instrument that automatically classifies the distributions of entities counted into clinical report-style categories: leukocytes, erythrocytes, and platelets [35]. With the incorporation of a laser in the fluidic system, this instrument also detects granularity of the cells measured, which allows it to further subdivide the leukocyte category into lymphocytes and granulocytes. A significant advantage for the Hemavet is its large linear range, which allow it to count crude cell preparations or cell separation outputs, in which the approximate cell concentration might be unknown, without the need to waste sample on determining an appropriate dilution factor. This method not only removed operator bias, but offered input flexibility and possessed methodological validation of an engineering standard that made it the most attractive choice for cell counting for this project.

Another method that is commonly used for cell counting but which was not used is flow cytometry, with counting beads. The flow cytometer fluidic system is tightly controlled and arranges cells in single-file order, which make it ideal for detecting cells in virtually any dilution; for those flow cytometers which do not actively measure volume of sample aspirated, counting beads of known concentration are spiked into the sample—the number of beads measured on a flow cytometry plot are then used to back-calculate

the cell concentration under the assumption that the sample is well-mixed. There does not appear to be an engineering standard written for this method, although in theory its accuracy should be comparable to that of electrozoning. For this project, the inconvenience of this method in addition to the lack of formal standardization was further justification: use of the flow cytometers for more complex experimental analysis took precedence over cell counting.

Microbubble counting

Equally important to establishing accurate cell counting was the microbubble count. It was important to reproducibly determine the ratio of microbubbles to cells mixed. However, as stated, the microbubbles were a heterogeneous distribution of sizes with the modal size being less than 2 microns. This makes most of the microbubbles difficult to see on a hemocytometer slide (with the need to contend with the varying size of the microbubbles adding additional effort to the counting procedure). Further, microbubbles are buoyant, causing them to rise to the top of the hemocytometer and effectively out of focus of the grid lines used for counting. As packaged from Targeson, the microbubbles were counted with a Beckman Coulter Multisizer Z4, providing a distribution a distribution of sizes from less than 1 micron to over 10 microns. This instrument was no longer available near the end of the project, but it was discovered that the bubbles were able to be counted using the Hemavet counter. As platelets are derived from fragmentation of a larger precursor cells, so microbubbles could be thought of as “cell fragments” for the purpose of counting. Sampling microbubbles on the Hemavet

and obtaining the resulting “platelet” category count showed linearity and consistency during serial dilution. Unfortunately, this workaround did not provide the distribution of sizes as the original Multisizer did. An unverified assumption therefore remains as to whether or not the microbubble size influenced its longevity in the particular storage and handling conditions for this project.

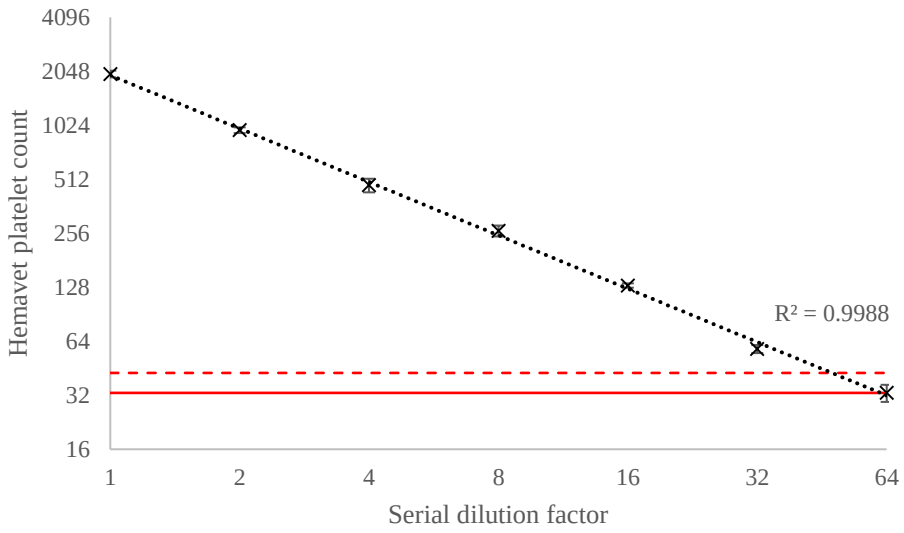

Figure 5. Microbubble counting linearity in serial dilution as measured by the Drew Scientific Hemavet. The microbubbles are counted as "platelets" by the instrument. The reported count is then matched with the Beckman Coulter Multisizer Z4 count on the same day. Subsequent counts on the Hemavet of microbubbles are correlated to this original count. Degradation of microbubbles is assumed to be uniform across all microbubble sizes and is numerically determined by simply comparing the Hemavet count over time with the original count. Red and dotted lines indicate detection limit and one standard deviation for the instrument.

Measuring cell proliferation

A common method for measuring cell proliferation in culture is to measure the dilution of a fluorescent dye that has been trapped inside cells that will undergo mitosis. For this project, the culture of 2D2 (cells from a transgenic mouse used to study experimental autoimmune encephalomyelitis—EAE—an animal model for multiple sclerosis) [36], OTII (cells from a transgenic mouse with CD4 T cells specific only to a peptide derived from ovalbumin) [37], P3 ($Apoe^{-/-}$ mice immunized with peptide of sequence SQEYSGSVANEANVY) [29], and wild-type C57BL/6 lymphocytes could be assessed with CFSE (carboxyfluorescein succinimidyl ester) or Cell Proliferation Dye eFluor450 (eBioscience, San Diego, CA). Before cells are initially plated, they are labeled with the dye, which is retained in the cell. A stained control that is not stimulated to proliferate serves not only as a negative control for the cell culturing and quality control for proliferation dye staining, but can also be used as a compensation control for flow cytometry. Cells that proliferate successfully dilute the proliferation dye with a factor of two each time division occurs. This process can be visualized as a series of discrete peaks that appear on a flow cytometry plot when the cells are analyzed. From right to left—the cells with the highest staining intensity to lowest—are cells which have progressively diluted the dye through division. The first peak, relative to the non-proliferatively stimulated control, represents cells which have not divided; the second peak represents one round of mitosis; the third peak two rounds, and so forth.

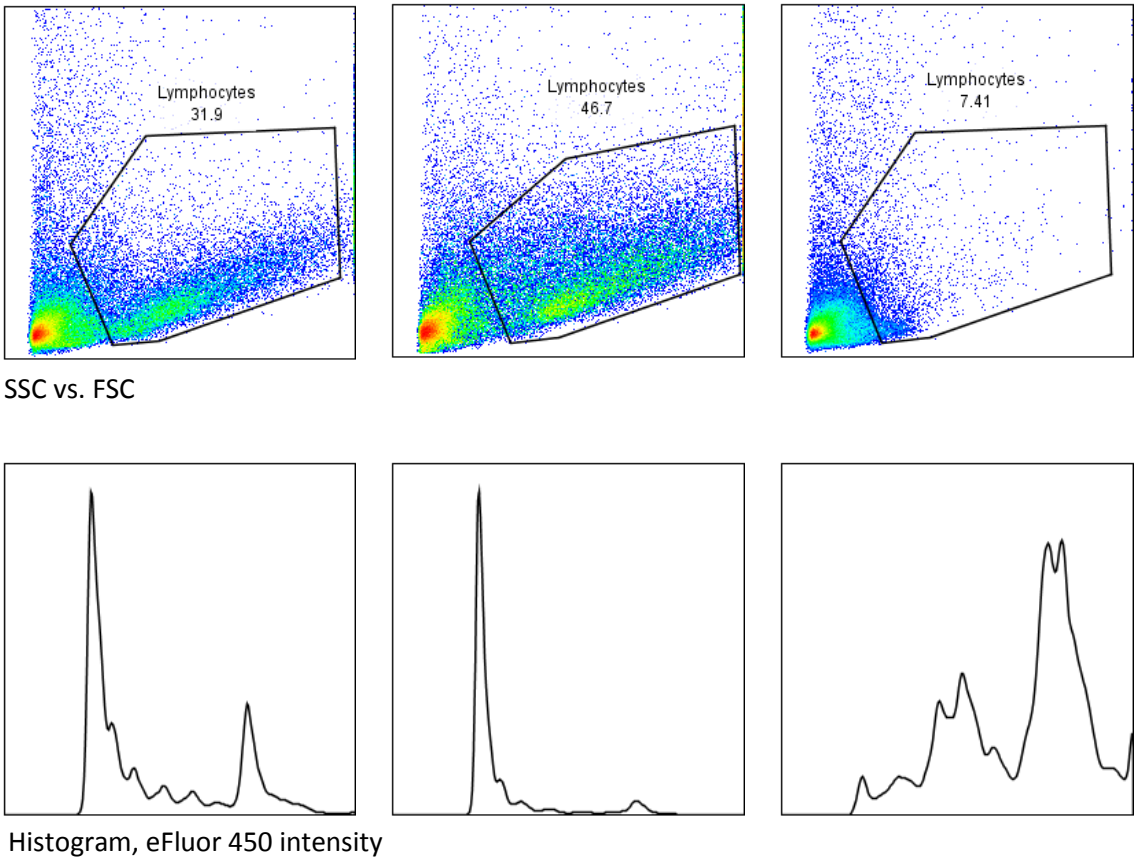

Figure 6. Example cell culture of OTII T cells. (top) Flow cytometry plots of cultured cells incubated with OVA peptide, left to right as low concentration, high concentration, and no peptide added. (bottom) Respective plots indicating dilution of proliferation dye.

Modeling

A simple model was made to describe the behavior of microbubbles. The freebody diagram of a microbubble consists of the buoyant and sedimentation (or gravitational) forces, in addition to a drag force during motion. The centrifuges used in this project were both fixed-angle and swinging-bucket style; due to centrifugation forces exceeding 200g, the effect of gravity during centrifugation was neglected. Differences in buffer density due to depth are negligible.

These forces could be summarized in an ordinary differential equation.

$$F = m\frac{dv}{dt} = \left(\rho_{bubble} - \rho_{buffer}\right)\left(\frac{4}{3}\pi r^3\right)C - F_d(v)$$

Here, v represents velocity, ρ is density, r is the radius of a microbubble, C is the centrifugal acceleration, and $F_d(v)$ is the drag force on the bubble, a function of its velocity. For low Reynolds number conditions and buffer of dynamic viscosity μ, then $F_d(v)$ for a sphere varies linearly with velocity:

$$F_d(v) = 6\pi\mu r v \qquad \text{(Stokes drag)}$$

Standard MATLAB ODE solvers can be used to numerically solve the resulting equation, thought it has a closed form solution. At terminal velocity, the drag term becomes zero and the equation further simplifies.

$$v_{terminal} = \frac{2\left(\rho_{bubble} - \rho_{buffer}\right)}{9\mu}Cr^2$$

Plots of microbubble position are as follows. The time-to-equilibration of forces acting on a microbubble is size-dependent, but all microbubbles approach terminal velocities at time scales very close (i.e., less than 1 microsecond) to the initiation of centrifugation. For estimation purposes, calculating traversing time of an exemplary bubble across the height of a column of liquid contained in a tube could be assumed to be at the terminal velocity. In practice, a well-mixed vessel containing microbubbles could be observed to settle at 1g over a matter of minutes; this is due to the large difference in density of the gas core of the microbubble versus the surrounding buffer. Settling of cells is much more gradual due to the cell's comparable density to that of buffers.

From these models, it could be inferred that most bubbles were too small to lift an exemplary lymphocyte on their own. Several smaller bubbles would need to attach to a given cell to provide the requisite buoyancy. Confocal microscopy data provided compelling visual support of these calculations.

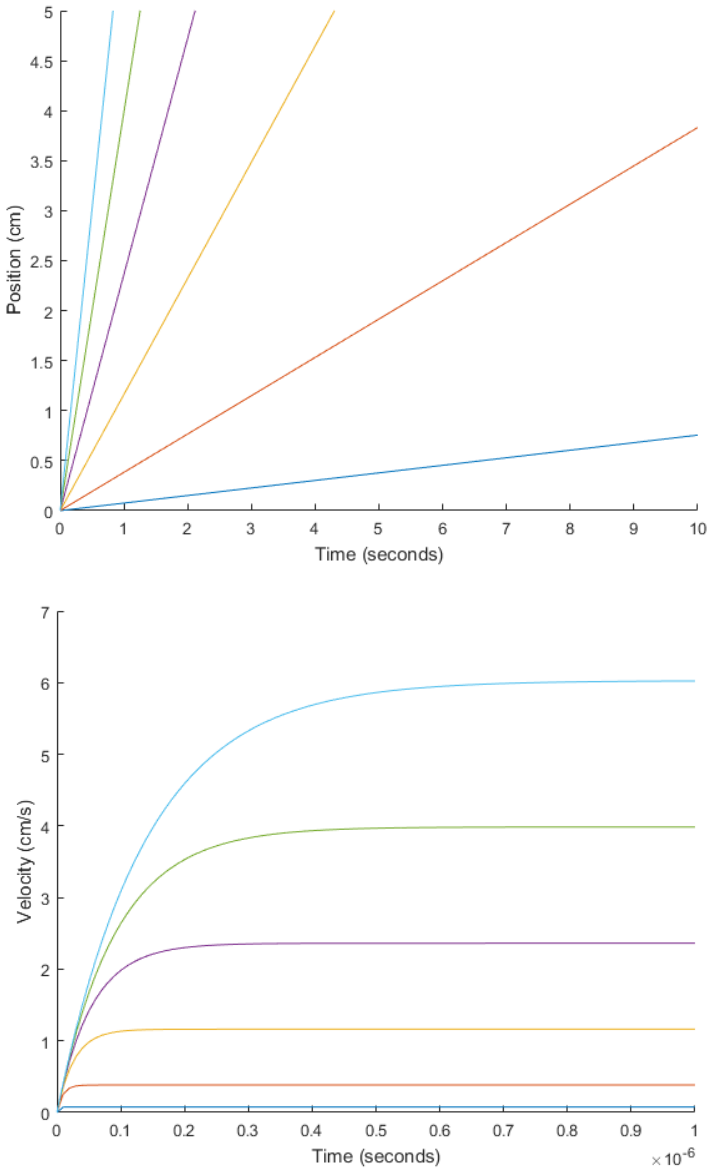

Figure 7. Position and velocity plots. (top) Position plots for experimental-scale time and distance. Curves from left to right correspond to decreasing microbubble sizes of approximately: 15, 12.2, 9.4, 6.6, 3.8, 1.677 (modal size) microns. (bottom) Corresponding velocity curves simulating microbubble centrifugation at 500g. Curve colors correspond to the top graphs; microbubble sizes decrease from top to bottom. Simulation assumes buffer density of 1000 kg/m^3, dynamic viscosity of 1.002 x 10^{-3} N/(m^{2}s), and perfluorobutane density of 11.21 kg/m^3.

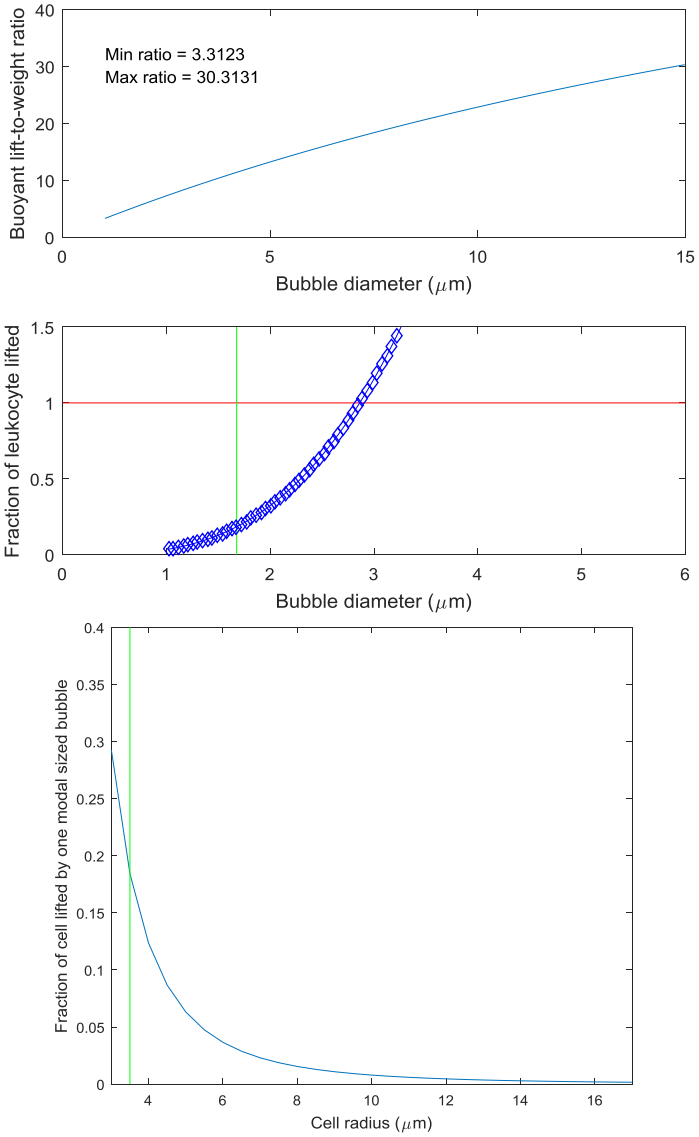

Figure 8. Buoyant lift capacity. (top) All microbubbles are subject to a buoyant force at least 3 times their weight. (mid) Percent of target cell lifted using materials properties for a generic leukocyte 7 microns in diameter and a single microbubble of varying size. Green indicates the modal diameter; red indicates 100% lift. (bottom) Power relationship for the lifting capacity of a single modal size microbubble. The lifting capacity is approximately 18.5% of a leukocyte 7 microns in diameter. Simulation uses previous parameters in addition to the following: leukocyte density of 1060 kg/m^3 and DSPC shell thickness of 50 nm (subtracted from total measured diameter) and density of 1106 kg/m^3.

Flow cytometry

This section provides a brief primer on flow cytometry for data shared later. The flow cytometer used was the Becton Dickinson LSRII (Franklin Lakes, NJ) with antibodies from various suppliers (Tonbo Biosciences, San Diego, CA; eBioscience, Inc., San Diego, CA; BioLegend, San Diego, CA; BD Biosciences, San Diego, CA). This instrument functions identically to the FACS sorting procedure described previously, except that the cells are discarded after analysis instead of sorted.

Some specificity controls are used in flow cytometry. First, compensation controls are required because the emission spectra of dyes used to label antibodies overlap. Modern flow cytometers equipped with 4 lasers can distinguish over a dozen different dyes at once. For compensation control, polystyrene beads are used that (some are coated with protein G) attach antibodies nonspecifically. The number of compensation controls used is dictated by the number of dyes used in the experimental staining panel. The need for compensation arises due to the wide emission spectra of fluorescent dyes—spillover, analogous to a falsely positive signal, into adjacent fluorescence-detecting photomultiplier tubes occurs. Through compensation, the percent of this spillover for every dye in the panel into all other fluorescence channels can be quantified and thus subtracted. Valid modern compensation is handled automatically by the acquisition software, though this does not absolve the user of making prudent dye selections to minimize spillover and preparing the compensation controls properly (they must possess fluorescence intensity equal to or greater than that of the brightest signal in the actual sample). These controls are dependent on the particular filter makeup of the instrument

used and its photomultiplier tube voltages; the controls must be set for every experiment. Compensation is required in any experiment involving two or more dyes, though the actual spillover between any two given dyes may be low or immeasurable. Flow cytometry panels used in this project typically exhibited less than 50% spillover.

Second, the fluorescence-minus-one (FMO) control is used. This is the best control for experiments in which more than two antibodies are used. A single FMO control for a given staining target is prepared by staining cells of interest with every dye in the staining panel except that dye for which the control is named. The maximum number of FMO controls is equal to the number of dyes used in the panel. During analysis, an FMO control then is used to determine the lower gating bound for its corresponding staining target: the logic here is that spillover from other dyes would increase the fluorescence intensity of the negative population relative to that of an unstained sample; by omitting the dye for the staining target, the appropriate boundary for the negative population can be drawn. This is a useful control for delineating positive events in a reproducible and quantifiably-justified manner, particularly if the events are not discretely resolvable by simple inspection (such as P6+ cells, which lie along a continuous range of staining intensity). FMO gates in this work were typically drawn using quadrant or quadrilateral gates tangent to the outward-most 5% of the total event population as visualized on a contour plot of the data. Because FMO controls are prepared using the sample of interest, not beads, they must be selected with care so as to not waste sample. Some FMO controls are superfluous in actual practice. For example, an FMO drawn on CD4 staining is unnecessary because CD4 staining is easily delineated

into discrete positive and negative events by inspection. To spare cells, the FMO control can be prepared from only a fractional aliquot of the total sample.

The third control is the isotype control, which may be combined with the FMO control to create a hybrid control. This control consists of staining cells of interest with an isotype-matched antibody labeled with the same fluorophore but which targeted an irrelevant antigen. The degree of staining was intended to indicate the level of nonspecific attachment. This control can reveal the degree of nonspecific antibody binding to Fc receptors found on myeloid cells.

The staining protocol for cells in this project evolved and depended on the experiments, such as the use of Fc receptor blocking reagent and staining temperature and duration. Initial titration experiments indicated a general range of antibody concentration for use (all concentrations likely saturated the cell surface antigens, but some provided better resolution of the positive and negative events due to reduction of the background nonspecific staining).

The analysis of flow cytometry data for this project is twofold. Becton Dickinson Diva software collected the data and provided basic analysis functionality to tune the instrument. Treestar FlowJo (Ashland, OR) software was then used for in-depth analysis and preparation of figures.

Cell separation with microbubbles

In brief summary, the microbubble-based cell separation protocol involves harvesting an organ of interest, typically spleen or lymph nodes, from the C57BL/6 or

Apoe$^{-/-}$ mouse. The organ is pressed through a 70 micron nylon filter into PBS buffer supplemented with 2% (v/v) fetal bovine serum to obtain a single cell suspension. In the case of splenocytes, the suspension is usually incubated with erythrocyte lysis buffer to rid the sample of red blood cells. The sample is then incubated with targeted microbubbles in a constant total volume (250 microliters) at room temperature for ten minutes in a cryovial mounted on an end-over-end mixer. The cryovial is rinsed and its contents transferred to a 5 mL FACS tube, which is sequentially centrifuged first for two minutes at 200g, and then for five minutes at 500g per Targeson protocol for maximum cell recovery [38]. Following centrifugation, a visible white layer called the cake forms at the air-water meniscus. The cake contains buoyant species: bubbles and attached cells, if any. As in conventional centrifugation, cells which have not been buoyed into this cake are sedimented into a pellet at the bottom of the tube; some cells adhere to the tube wall. The cake and pellet fractions typically form visibly discrete sections on the containing FACS tube. Next, the cake is locally resuspended into solution by gentle tapping on the nearest part of the tube. It can then be separated from the pellet by decanting the liquid fraction in one motion into a different container, usually a 15 mL Falcon tube. Finally, the microbubbles can be imploded (crushed) by pressurization to two atmospheres. In this project, crushing was usually accomplished by inserting the plunger of a 10 mL syringe into the 15 mL Falcon tube until the air volume was halved. Subsequent microscopy of crushed cake fractions confirms the destruction of the microbubbles, shown later. Both the pellet and cake fractions could then be used for downstream purposes, though in this project they were always prepared for flow cytometry at this point.

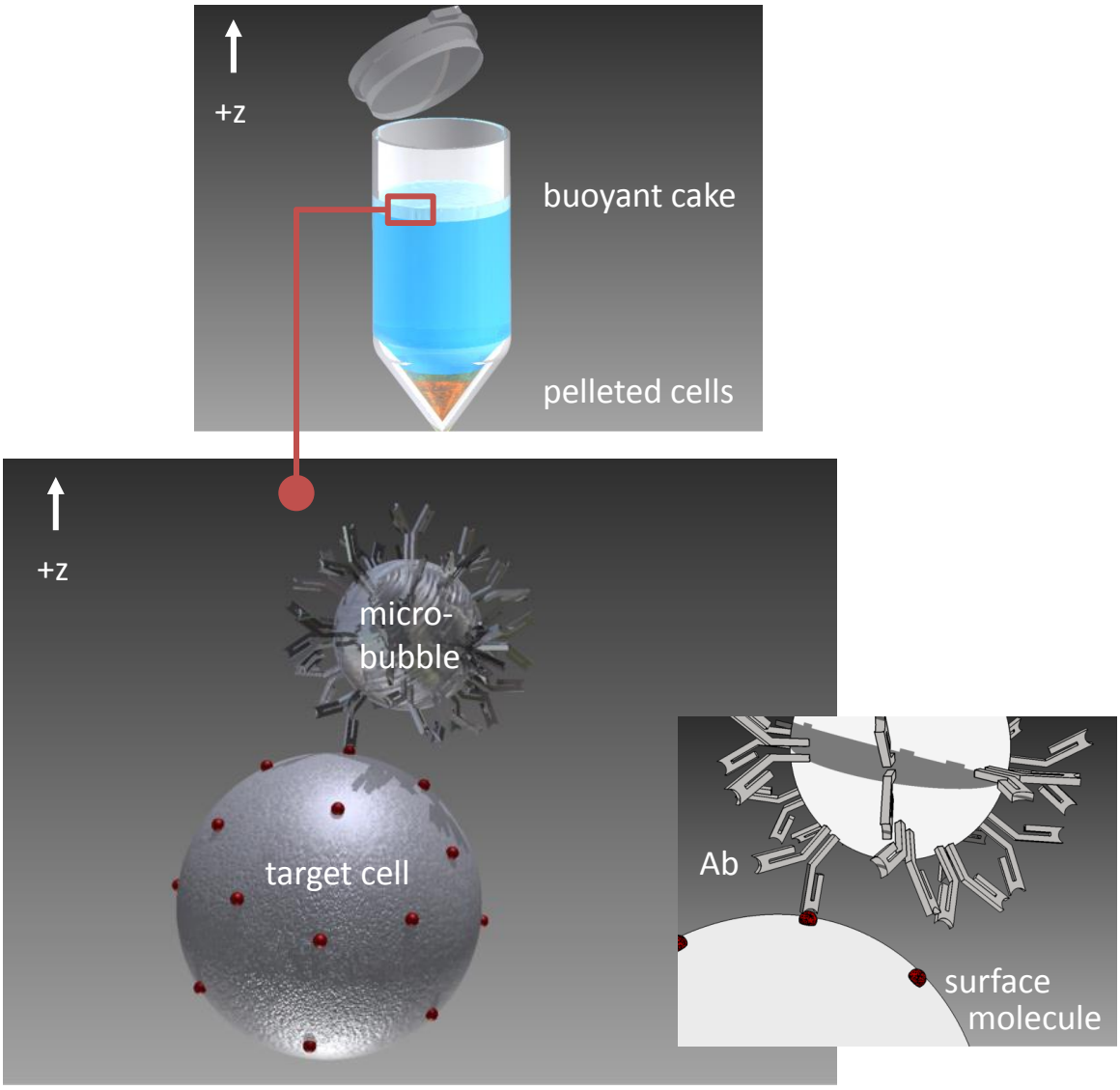

Figure 9. Schematic overview of microbubble-based separation, showing buoyant cake containing microbubbles and target cells.

Cell separation devices

Before the decanting method was used to separate the cake and pellet fractions, pipetting was used to remove the cake fraction manually through aspiration alone, but this method proved to be variable. Therefore, some effort was expended into creating a device that could cleanly separate a column of liquid into two discrete components. Five attempts were made. All functioned on the principle of creating a pendant droplet in the interstitial liquid separating the cake and pellet: following centrifugation, this area should be free of cells. A pendant droplet is created when a drinking straw is removed from liquid with the opposing end of the straw capped. The combination of surface tension and pressure differential created in the sealed end of the straw relative to the surrounding atmosphere as the liquid column begins to move downward keeps a droplet suspended at the open end of the straw. Removing the cap equalizes the pressure and the liquid moves out of the straw. Critical parameters for pendant droplet formation include the diameter of the straw, and the viscosity of the contained liquid. These factors affect surface tension.

The first attempt was a 50 mL Falcon tube-sized device made of several components. All were machined by a Campus Research Machine Shop (University of California San Diego, La Jolla, CA) machinist from polyoxymethylene thermoplastic stock material (Delrin) for low adhesion character. The components could be assembled into two different configurations: pendant/capture and crush. In the pendant configuration, a heterogeneous mixture of microbubbles and cells could be loaded into the central bore of the assembly, spanning two separate components that could thread into each other, and sealed together by means of an o-ring. Threaded and o-ring features and

some part tolerances were designed as per engineering guidelines in Machinery's Handbook [39], and the CAD model and 2D schematics for machining were created in Autodesk Inventor. This design did not perform better than manually pipetting the cake fraction away. The precise reason was not fully explored, but the device suffered from intermittent leaks, resulting in loss of sample; unscrewing the components seemed to perturb the pendant drop; solution viscosity was not accounted for in initial calculations (water was used as an approximation); and the device was not designed to be sterilized in an autoclave, necessitating lengthy and inconvenient cleaning in between samples. Subsequent iterations of this design would be well-advised to err on the side of smaller column diameter, as it is obviously not possible to return material to a hole once it has been removed by machining. With the advent of 3D printing technology, different cross-sectional patterns, otherwise impractical to conventionally machine, might be attempted to optimize surface tension as well. Ultimately, the loss of valuable sample precluded further study of the device.

The second through fifth attempts were miniature versions designed to fit into a standard tabletop centrifuge accommodating standard 2 milliliter-sized Eppendorf tubes, typically with a fixed-angle rotor. They were intended to use sufficiently small quantities of manufacturing material so as to be disposable, obviating the need for decontamination. Due to the high cost of injection molding, Stratasys (Stratasys, Ltd., Eden Prairie, MN) and MakerBot Replicator 2 (MakerBot, New York, NY) printers were used to 3D print the prototypes using polylactic acid (PLA) filament. Designs two through four were variations on producing a pendant drop on an interior component that was sheathed by an exterior shell: the cake fraction was intended to be separated away from the pellet by

capping the interior component with a finger and sliding it away slowly from the exterior shell. Designs two and three functioned on the sliding principle and were produced on the two different printers with slightly varying tolerances. Design four consisted of threaded features that would allow the two components to be unscrewed from each other. Design five was a tapered tube intended to sediment pelleted cells into a small section of the device which could then be twisted off with standard pliers; the tapered design also meant to more cleanly pellet cells into a concentrated mass instead of allowing them to be streaked across part of the length of the tube due to the rotor angle of the small centrifuges. None of these designs were tested after initial prototyping failures from leaks, due to time and material constraints.

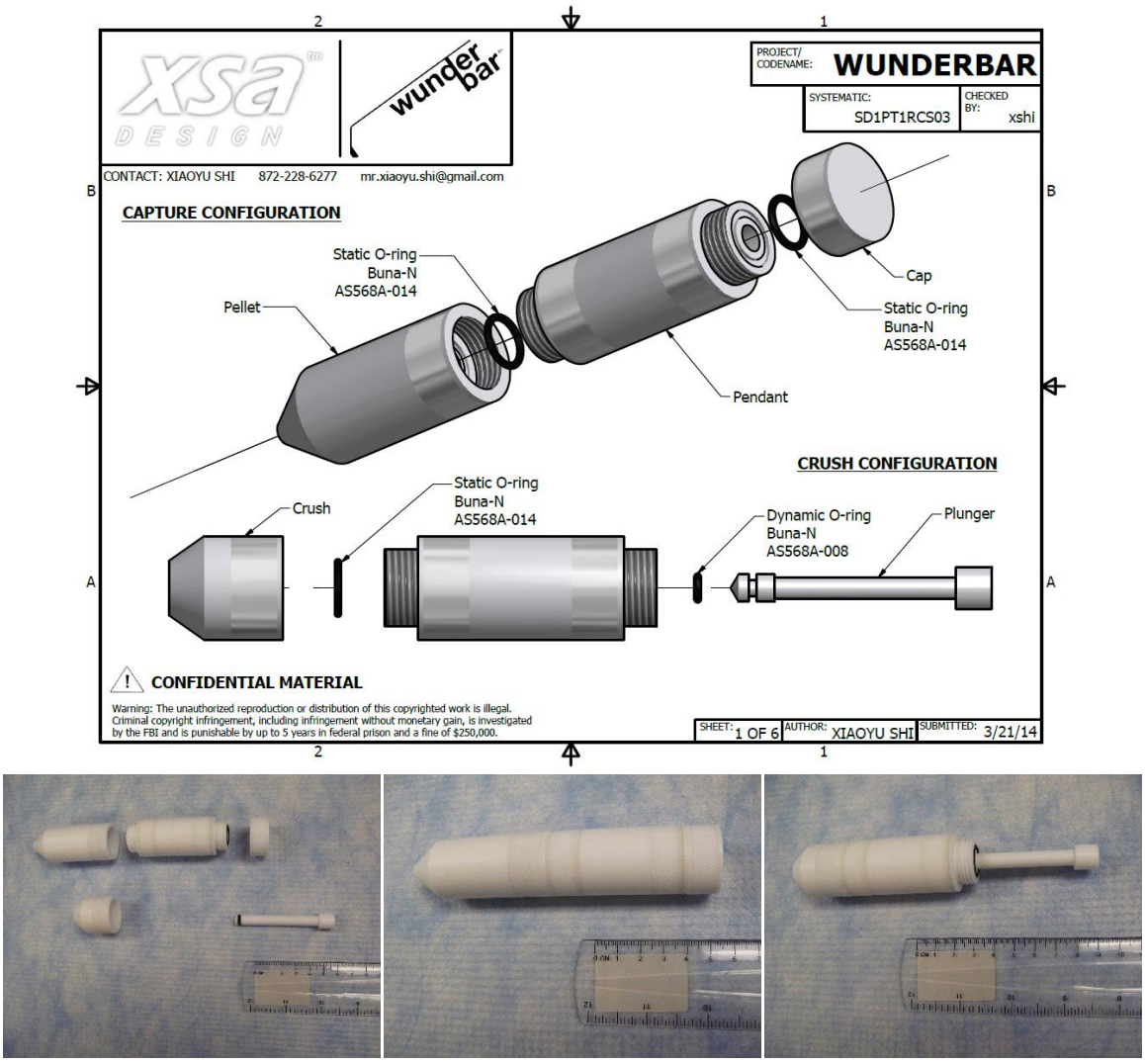

Figure 10. First microbubble separation device. The bore was machined through the entire length of one component and partially into another; the liquid level was to fill the entire latter component and partially fill the former; the latter component was intended to contain the pelleted cells. Following centrifugation in a standard tabletop centrifuge able to accommodate a 50 mL Falcon tube, as the cake and pellet fractions separated, a threaded cap could be placed on top of the uppermost component. An o-ring immediately underneath the cap provided the requisite seal for the pendant drop. Then, as the separation point of the two components of this configuration was at an intermediate distance in between the cake and pellet, the two components could be separated, one component cleanly holding the cake fraction, suspended above a pendant droplet, and the other component containing the pelleted cells. Next, in the crush configuration, the component holding the cake fraction was threaded onto another bottom component, again sealed with an o-ring. The cap was removed and a custom plunger was used to crush the microbubbles and release the cells, which then could also be pelleted and collected.

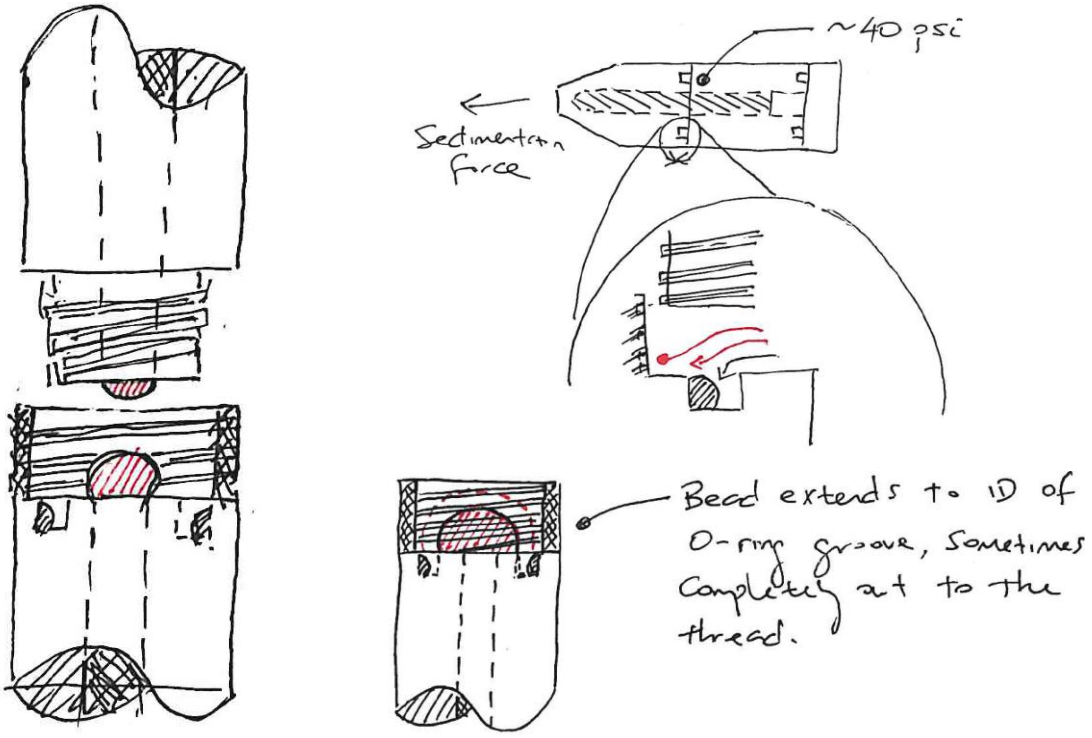

Figure 11. Separation device failure. Left diagram shows intended drop formation as pendant and pellet sections were separated. This was not reliable, and liquid leaked past the o-ring groove.

Figure 12. Second through fifth devices, top to bottom.

Though these devices were unsuccessful, a custom centrifuge adapter specifically designed to accommodate the gamut of tube sizes used in the microbubble separation protocol was successfully printed in acrylonitrile butadiene styrene (ABS) filament using an AirWolf AXIOM (Airwolf 3D, Costa Mesa, CA) 3D printer over the course of 63 hours and 19 minutes. A subsequent print of the corresponding balancing adapter was performed in the same amount of time and within 3 grams of the first adapter. This adapter can accommodate standard 15 and 50 mL Falcon, 5 mL FACS, and lip-hanging 0.6 mL, 1 mL, and 2 mL Eppendorf tubes and is intended for use in the Sorvall Legend RT swinging-bucket centrifuge. The adapter can be chilled and otherwise used to carry many disparate tubes. Basic finite element analysis (FEA) was performed using built-in simulation software to the Autodesk Inventor CAD program to assess survivability of the apparatus during centrifugation at 800g, with all available bores filled to capacity with the maximum amount of liquid water. Tube weights were neglected. The default material of isotropic ABS was used in the simulation, which does not reflect the anisotropy of the 3D printing process—additionally, the printer was configured to print solid spaces with 10% hollow volume. The appropriateness of the assumption of isotropy was not explored, but using this assumption nonetheless, in addition to the default use of the von Mises failure criterion [40], leads to a relatively high factor of safety of tensile and compressive loading. Cycling loading, off-balanced loads, incomplete loading, and combinations thereof were not considered.

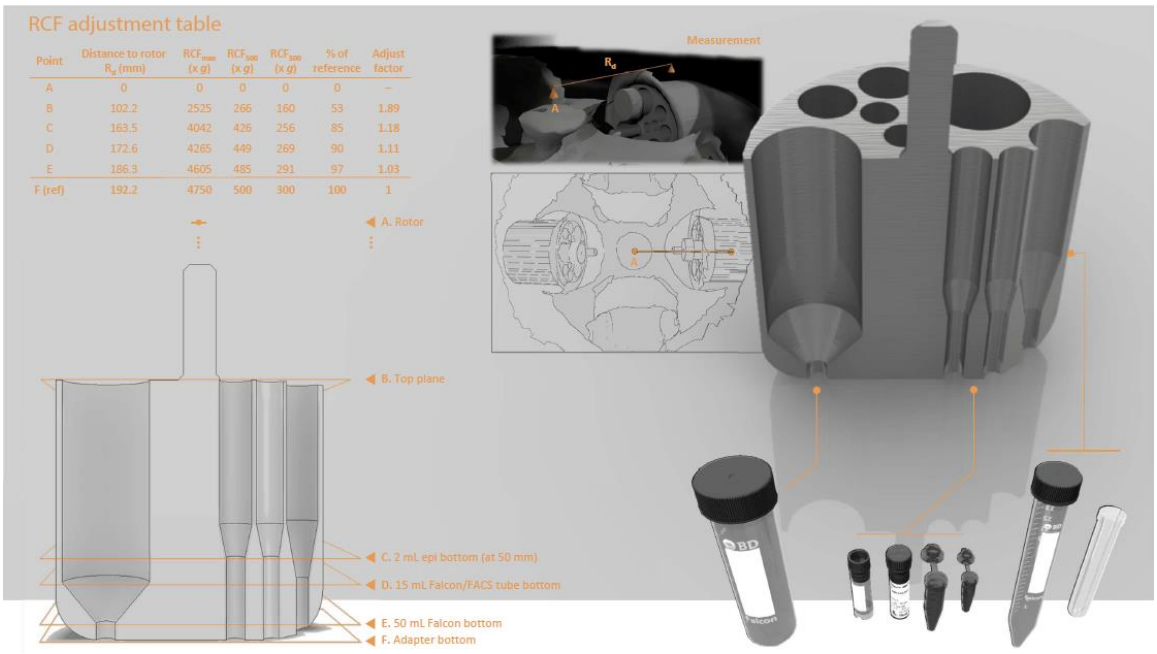

Figure 13. Combination adapter for the Sorvall Legend RT swinging bucket centrifuge. Designed to accommodate all tubes needed for the cell separation protocol without requiring adapter swapping. Actual centrifugal force at the tip of each tube.

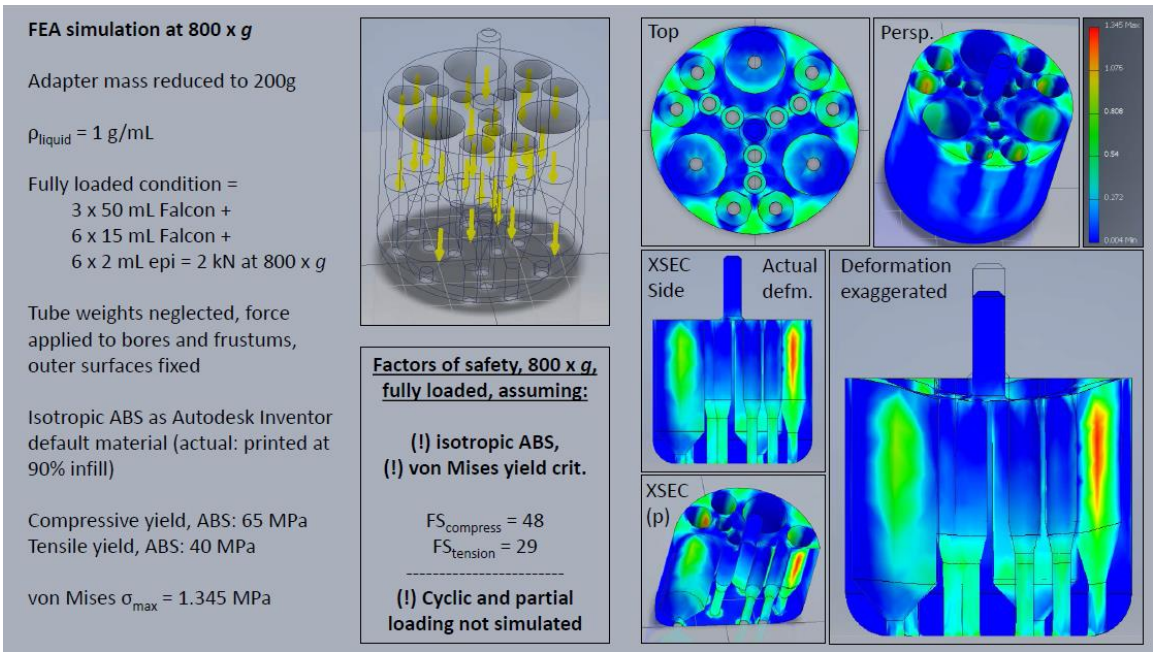

Figure 14. Finite element analysis of adapter centrifugation at 800g.

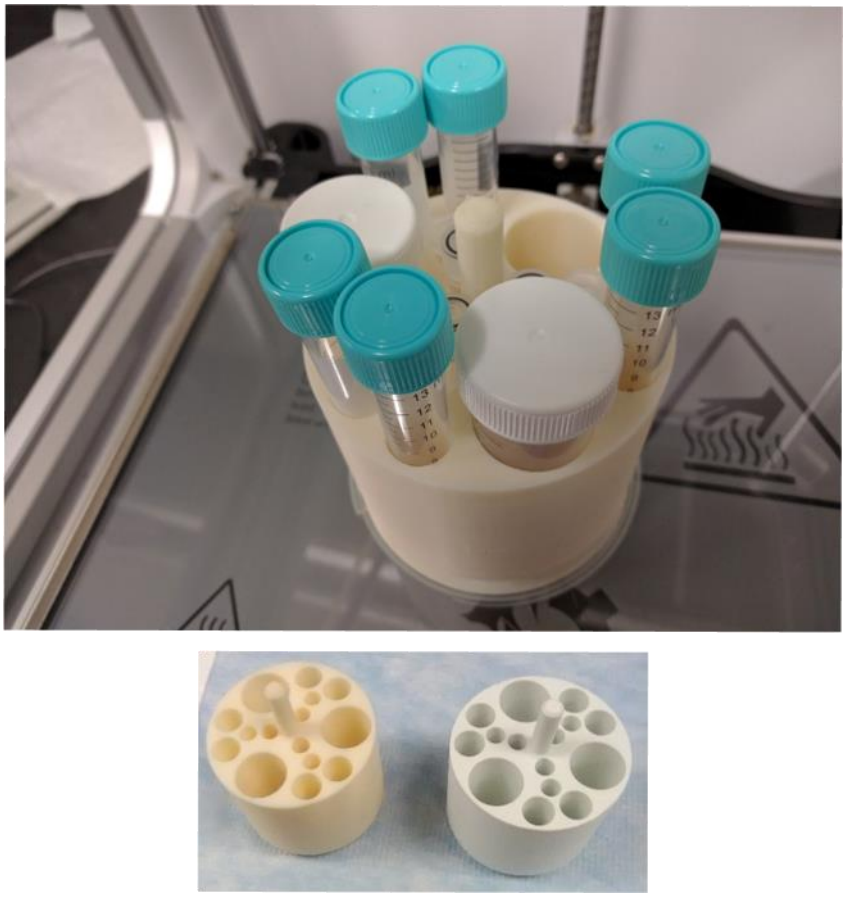

Figure 15. 3D printed combination adapter.

B cell separation

Cell separation with microbubbles was initially performed with B lymphocytes as the target. The microbubbles used were covalently conjugated by Targeson to anti-CD19 antibody. Commercially available fluorescent monoclonal antibodies attach to the same epitope on the CD19 molecule; the antibody used for separation blocks antibodies that would be used for CD19 detection by flow cytometry. Thus, the B220 surface receptor was chosen as a surrogate target for flow cytometry staining. Correlation between the two markers was assessed in Figure 16. Representative histograms of the resultant separation are shown in Figure 17; purity of the separations was generally high.

Preliminary phenotyping was also performed on C57BL/6 splenocytes to determine the nature of cell populations present in cell preparations for separation.

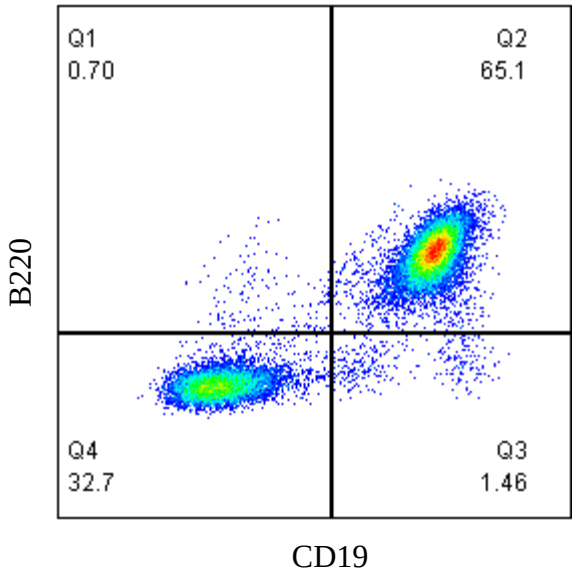

Figure 16. Correlation between splenocyte B220 and CD19 markers. Approximately 65% of cells are consistently stained in doubly- and singly-stained samples.

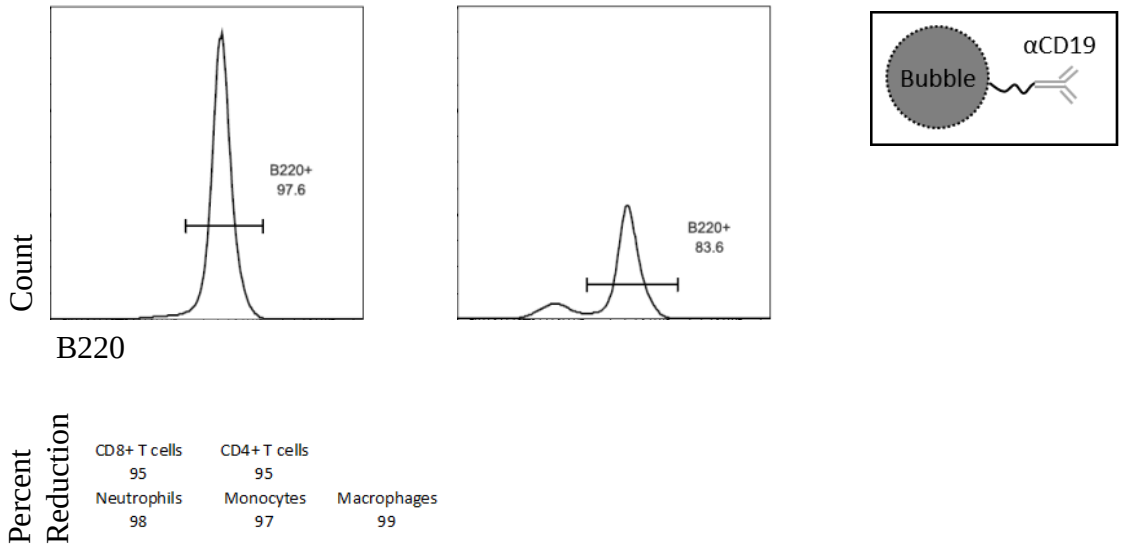

Figure 17. B cell separation representative plots. (left) B220+ cells in the buoyant cake versus leftover in the pellet (right). (bottom) Reduction of contaminating cells following separation, expressed as cake-to-pellet percent; calculated from absolute cell numbers.

Following B lymphocytes, separation of CD4+ T lymphocytes was attempted. The microbubbles used for these separations were not covalently linked to antibody; instead, the Targestar-SA streptavidin microbubble was used, consisting of streptavidin molecules covalently linked to microbubbles through polyethylene glycol (PEG) linkage. The streptavidin microbubble was then incubated with biotinylated CD4 antibody to create a bubble construct that could attach to the target cell of interest. CD4 T lymphocyte separation was used as a setup experiment for antigen-specific CD4 T cell separation.

As noted, the antigen-specific CD4 T cells of interest in the C57BL/6 mouse are reactive to a self-peptide known as P6 (sequence: TGAYSNASSTESASY).

Assessment of separation

Important metrics for separation quality for this project include yield, purity, and technical loss. The input for separation is defined as the number of target cells present in the cell suspension used as a starting point for separation. For example, the input for a CD4 T cell separation is 1 million cells if 10% of a total mixture of 10 million cells is used.

Purity refers to the percentage of target cells in the harvested fraction, as determined by staining for flow cytometry. Table 3 defines harvested fractions.

Yield refers to the number of target cells in the harvested fraction divided by the number of target cells in the input. In this project, an aliquot of cell suspension is counted and analyzed by flow cytometry without undergoing separation to determine the

theoretical number of target cells that are available in the sample. Because the microbubbles were not optimized as a commercial separation product, the main focus of evaluating separations was directed towards purity of separations. Indeed, yield for some separations were quite poor (around 10%).

Technical loss refers to all cell losses as a result of the protocol, including pipetting error, centrifugation loss from aspirating supernate, cell adhesion to containers, and losses due to the separation technique. Technical loss is a conservation equation. It is derived from summing the total number of cells in the positive and negative fractions and comparing this total to the total input number of cells. Technical loss may alternatively be measured by applying the same analysis to target cells instead of total cells to determine if target cell loss was not representative of total cell loss.

Table 3. Definition of harvested fractions.

Method	**Selection**	**Harvested fraction**
Microbubble	Positive	Cake
Microbubble	Negative	Pellet
Magnetic bead	Positive	Magnet or column
Magnetic bead	Negative	Flow-through

Mice

Wild-type and Apoe-/- C57BL/6 mice (Jackson Laboratory, Bar Harbor, ME) were used in this project. The ApoE knockout has a defect in cholesterol transport which increases its susceptibility to atherosclerosis. All mice were killed by CO_2 asphyxiation per listed La Jolla Institute Division of Laboratory Animal Care protocol prior to any experiment. A secondary method was always used to ensure death, and was either cervical dislocation, removal of sufficient blood by cardiac puncture, substantive cutting into the peritoneal cavity, or a combination of these methods. Subsequently, the spleen was removed and/or a pooled combination of the following lymph nodes (as many as could be readily located): cervical, deep cervical, brachial, axillary, mesenteric, inguinal, sciatic, lumbar, and sacral. These organs were prepared into single cell suspensions for experiments as previously described.

Microscopy

Fluorescence microscopy was used to visualize cells and microbubbles. This technique is an "orthogonal" method that was valuable because it provided visual confirmation of separation. Labeling proceeded similarly to staining for flow cytometry with minor adjustments such as increase in staining time and addition of reagent to limit dye bleaching for exposure to the excitation source. This is because detection instrumentation for microscopes is not as sensitive as those used in a flow cytometer. Fluorescent events detectable at the lower limit for flow cytometry could be effectively invisible to a microscope.

Two strategies in this project to label cells and microbubbles were to label with fluorescent antibodies or to label with lipid membrane dyes. Fluorescent antibodies consisted of those attaching to cell surface markers, such as the CD4 receptor, or attaching to entities on microbubble constructs, such as the biotinylated MHCII monomer. DiI and DiO are lipid membrane-staining dyes that were originally used, but the staining intensity and variability were inferior to that of antibody labeling.

Brightfield and epifluorescence microscopy were used before acquiring the bulk of the data on the Leica SP5 laser scanning confocal microscope. The confocal microscope allows for visualization of a single focal plane, resulting in increased resolution.

CD4 separation construct

This set of experiments was intended to evaluate the effectiveness of the streptavidin microbubble in attaching biotinylated CD4 antibodies and separating CD4 T cells as a setup experiment prior to separating antigen-specific CD4 T cells. Microbubbles and biotinylated CD4 antibody were incubated at room temperature per an adapted protocol from Targeson to prepare the separation construct. The construct was then mixed with cells and the separation performed as described previously. The antibody used when this separation construct was compared to a commercially available kit (eBioscience MagniSort) is identical to the one contained in the kit.

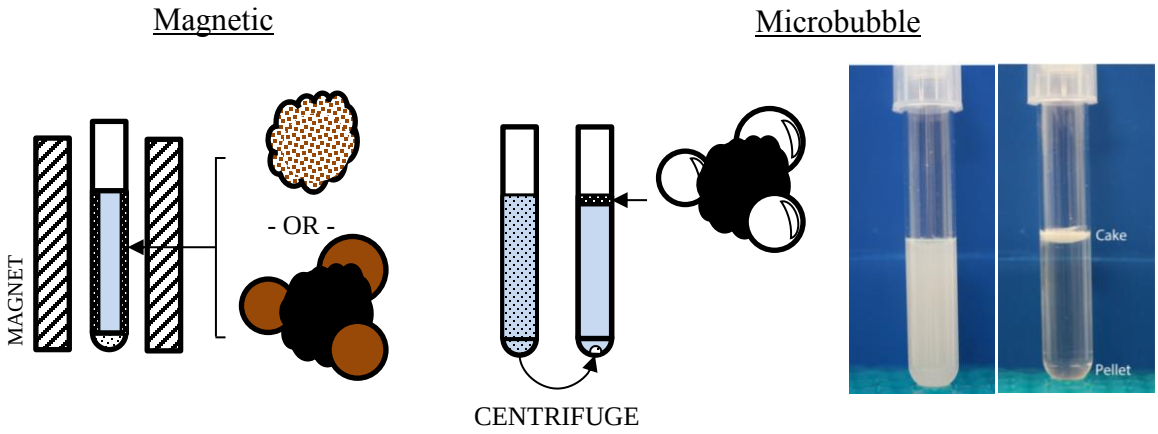

Figure 18. Bulk enrichment of cells using two methods. (left) Magnetic beads. Large micron or small nanometer-scale iron oxide particles, shown in brown, attach to cells of interest in a positive selection protocol. Separation is achieved by inserting the tube into a magnet (cross section shown). The radial magnetic force pulls cells to the circumference of the tube. Unattached cells are eliminated by decanting the tube while still in the magnet. (right) Microbubbles. Lipid microparticles filled with fluorocarbon gas buoy attached cells to the top of the tube during centrifugation. Unattached cells pellet to the bottom. Both separation constructs rely on surface conjugation of the streptavidin molecule, either prepared with an excess of biotinylated anti-CD4 antibody (bCD4), washed, and then incubated with cells, or mixed with cells that have already been incubated with anti-CD4 antibody. Thus successful separation depends on this streptavidin-bCD4-CD4 linkage between a microbubble or magnetic bead and a target cell. Use of a different biotinylated species in place of bCD4 makes the method versatile. Actual cake and pellet fraction shown; image from Targeson.

Confocal microscopy was performed to confirm the separation. Ibidi (Madison, WI) flow chambers and a custom polydimethylsiloxane (PDMS) single-channel flow chamber held in a custom 3D printed holder were used in epifluorescence microscopes before a simple solution was developed to address the problem of unwanted flow: a coverslip sandwich consisting of two #1.5 rectangular microscopy slides with two #1 coverslips inserted as spacers (dimensions shown on Figure 20). When a mixture of microbubbles and cells was placed in the sandwich, the spacers held the two slides apart at a distance of around 200 microns, providing a chamber in which floating and sedimenting species could be resolved. For microscopy, microbubbles were stained with a fluorescent IgG secondary antibody and washed prior to mixing. Cells were stained with anti-TCRβ due to cross-reaction of commercially available CD4 antibodies. The coverslip sandwich could be placed into a 60 mL syringe (Becton Dickinson) and the plunger pressed to the graduations' halfway mark to crush the microbubbles. The coverslip sandwich could then be quickly replaced on the microscope to watch the bubbles falling over time.

Flow cytometry of the separation was also done to confirm separation with another method. The cake fraction of the separation is enriched for CD4 T cells.

The microbubble CD4 separation construct was compared with a commercially available CD4 positive selection kit from eBioscience in Figure 18. The commercially available kit performs better than the microbubble separation construct.

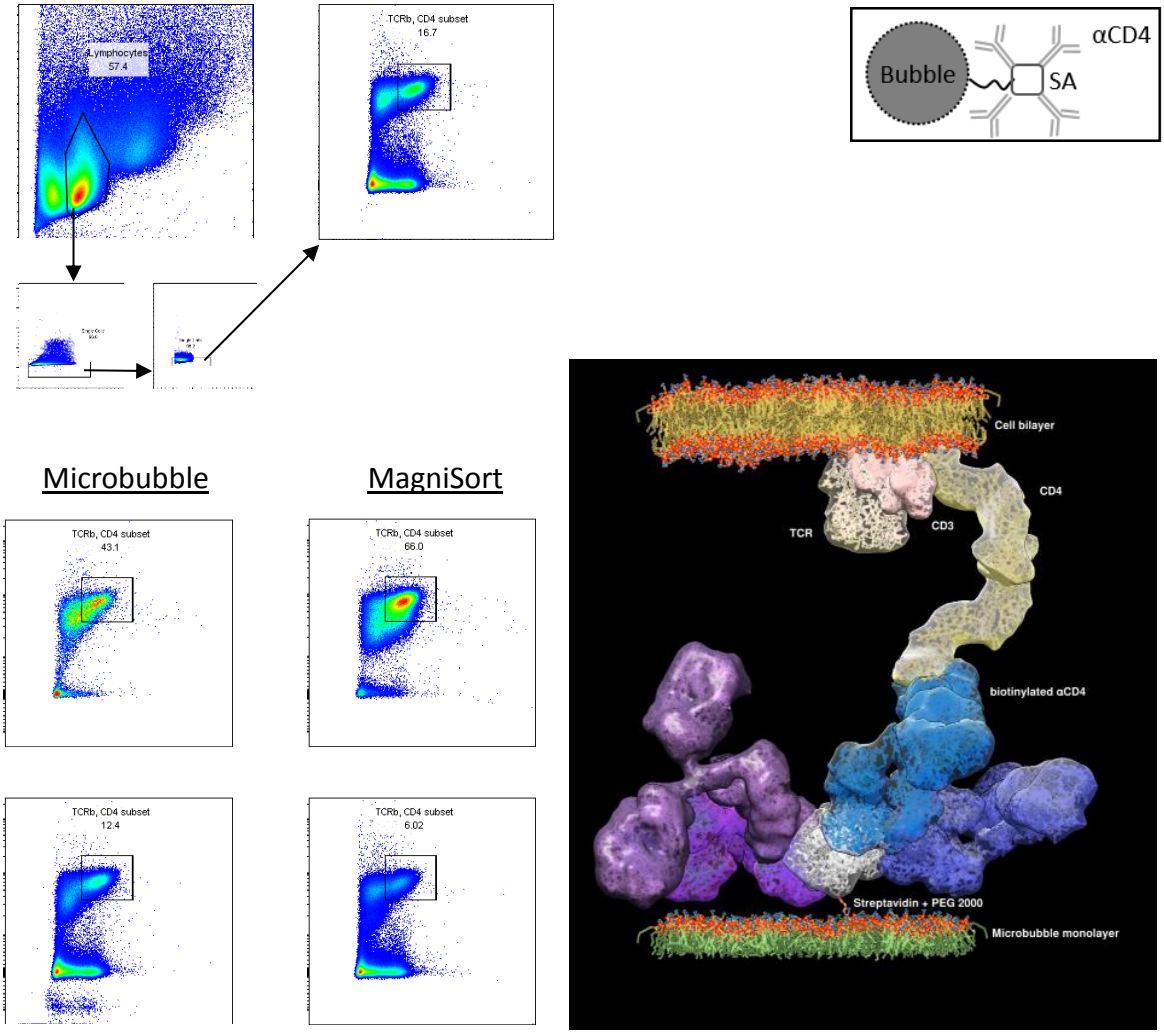

Figure 19. Comparison of the eBioscience MagniSort positive selection kit versus streptavidin-biotinylated CD4 microbubble construct. Both separation methods use the same biotinylated CD4 clone. (top) Representative gating scheme for singlet CD4+TCRβ+ lymphocytes (light scatter > singlets > singlets > TCRβ+CD4+). The biotinylated CD4 antibody is non-blocking. (bottom left) Comparison of yield and purity for the two separation methods. Top plot set is the positively selected CD4 fraction in the cake and bead-bound fractions; bottom set is the pelleted and flow-through fraction for each separation method. Microbubble separation has lower purity and yield than the commercial kit. (bottom right) CD4 microbubble separation construct rendering created using UCSF Chimera; credits shared with Figure 3.

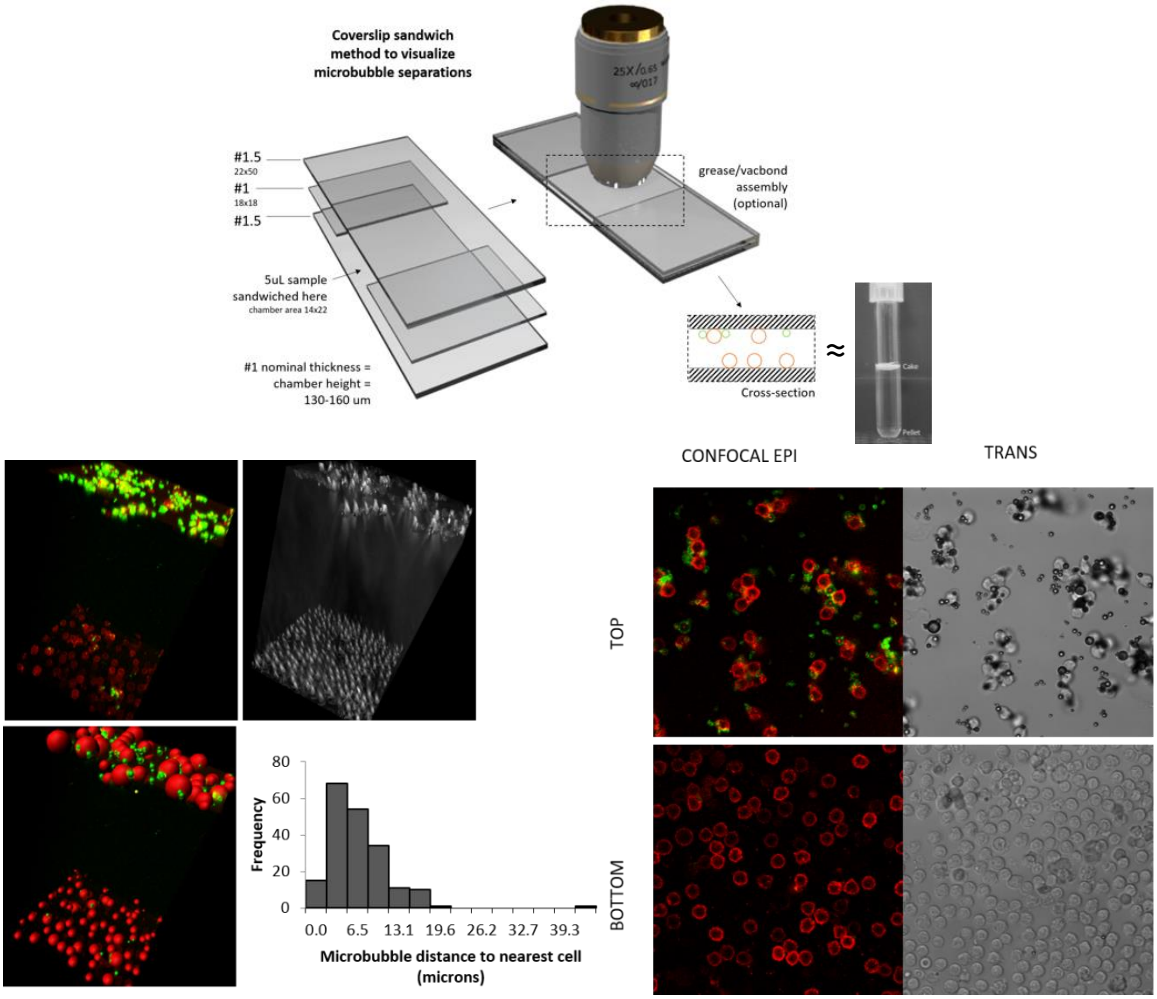

Figure 20. Confocal visualization. The Leica SP5 laser scanning confocal microscope was used to image microbubble mixtures. (top) Coverslip sandwich. This setup used coverslips as spacers to create a simple chamber at the appropriate distance to visualize buoyant and sedimented cells at two discrete focal planes. (bottom right) Streptavidin-conjugated microbubbles were incubated with biotinylated CD4 antibody and then single-cell suspension preparation of pooled lymph nodes (of those available from inguinal, mesenteric, sacral, lumbar, brachial, axillary, cervical regions) from a WT B6 mouse. Cells are stained with TCRβ fluorescent antibody (AF647, red). The streptavidin-bCD4 microbubble separation construct is stained with IgG secondary antibody (AF488, green). Left micrographs are fluorescence channels; brightfield signal is right. Top image set is the focal plane corresponding to the top of the coverslip sandwich; sedimented cells are in the bottom images. (bottom left) Imaris reconstruction. Z-slices of the chamber were used to create 3D reconstructions of the transillumination and fluorescent signals. Surface modeling was derived from the fluorescence signal and used to calculate average bubble-to-cell distances using the Imaris (Bitplane, South Windsor, CT) built-in distance transform function. The distribution follows the size distribution of microbubbles, as would be expected.

Detection of antigen-specific CD4 T cells

Due to the low affinity of a single MHCII-TCR attachment, biotinylated MHCII molecules are multimerized into dextramers or tetramers to allow multiple low affinity attachments to interact, reminiscent of the cumulative effect of multiple low-strength attachments.

Tetramers were originally tried, produced by the Marc Jenkins lab of Minnesota before dextramers were exclusively used.

P6 MHCII separation construct

This was the ultimate goal of the project. Preparation of the construct, separation, and microscopy and flow cytometry were performed analogously to the CD4 separation protocol. As the biotinylated MHCII monomer possesses a molecular weight comparable to that of an antibody, the preparation step was not adjusted to compensate for attachment of this different species.

Ideally, the separation construct could be removed from the target cell following separation and when the microbubble was crushed, but this was later shown to not be the case. The microbubble has an unknown number of attached streptavidin molecules. It was assumed to be much greater than that of a dextramer (12-20) of tetramer (4). Thus, the microbubble construct would in theory interact with cells with a higher valency as a result.

Experiments indicated that some separation construct remnant remained attached to the target cells following bubble implosion. This was indicated by MHCII antibody

staining, which was still present on the separated cells, pointing to the presence of MHCII epitopes. It was theorized that the MHCII monomers form tetramer-like entities at each streptavidin molecule of the microbubble, which would then resist detachment from the cell even after microbubble implosion. Initially, an attempt was made to address this by creating a titrated separation construct. This involved titrating an amount of an irrelevant biotinylated antibody, TER119 (an erythrocyte marker), along with biotinylated MHCII monomer in the preparation of the microbubble construct and prior to incubation with cells. The idea was that each streptavidin molecule would then be attached to at most a single MHCII monomer. This construct did not appear to separate cells reproducibly and was abandoned, although I believe it merits additional attempts.

The separation construct ultimately used was not titrated against irrelevant biotinylated antibody.

Separation is shown by flow cytometry to enrich cells. The fold enrichment differs based on MHCII staining versus P6 MHCII dextramer staining.

Microscopy was performed to visually confirm separation of the cells on two discrete focal planes, with microbubbles attached to cells appearing on the top plane, and sedimented cells appearing at the bottom. The implosion experiment was performed as well to confirm that the buoyant cells would fall following microbubble implosion. Interestingly, this experiment also confirmed that some cells had microbubbles attached that were too small to lift the cell, which was predicted by earlier modeling.

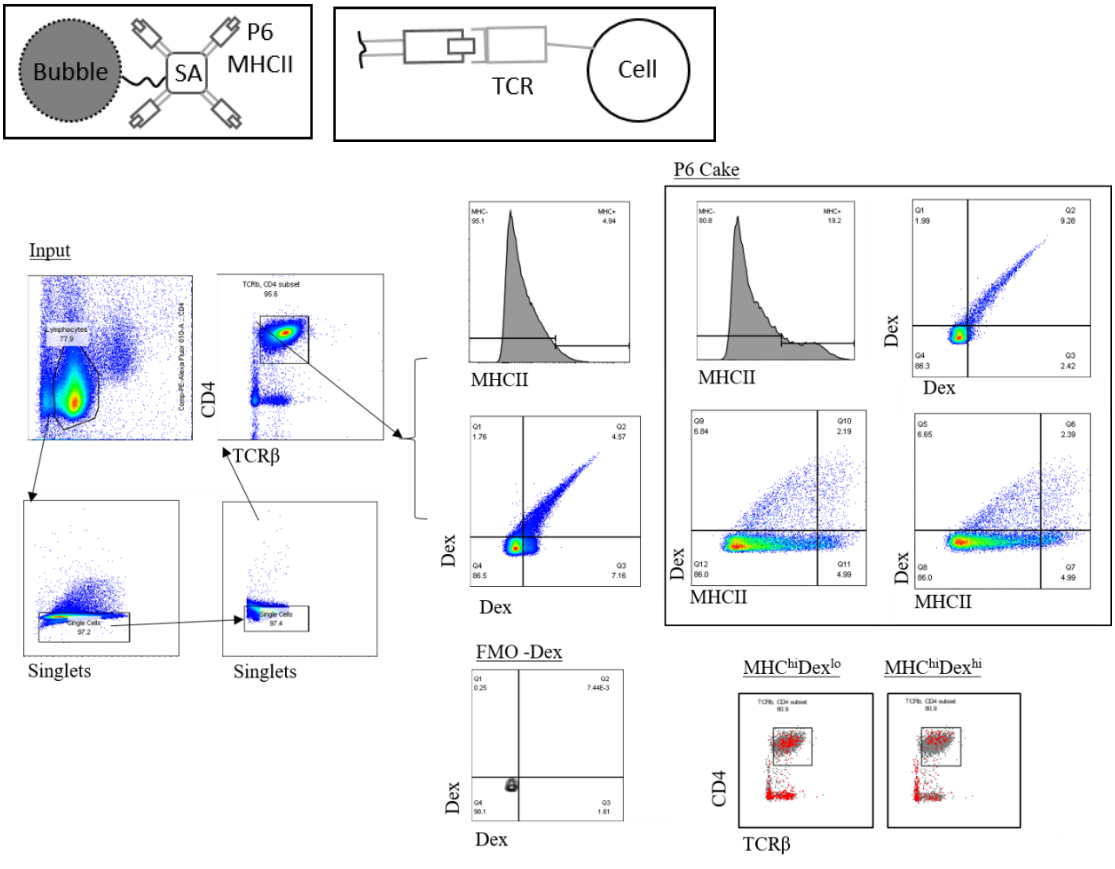

	P6 Construct		Input		Fold increase
n	MHC+	Dex+	MHC+	Dex+	MHC+
1	19.2	9.28	4.94	4.57	3.9
2	32.3	4.02	5.13	0.69	6.3
3	21.2	5.09	4.93	1.86	4.3
Mean	24.2	6.1	5	2.4	**4.8**
sstdev	7.1	2.8	0.1	2	**1.3**
%CV	29.1	45.3	2.3	83.9	**26.7**

Figure 21. Separation of antigen specific P6 T cells using a streptavidin-biotinylated P6 MHCII microbubble construct in a positive selection protocol. The construct is prepared by adding excess biotinylated P6 monomer to streptavidin-conjugated microbubbles, followed by addition of fluorescent anti-MHCII antibody. Input cells are pre-enriched with a custom CD4 negative selection kit. Following bubble separation, cells are P6 dextramer stained. (top) Schematic of separation construct. (mid) Representative gating scheme for singlet CD4+TCRβ+ lymphocytes and gating bounds for P6+ cells by dextramer double FMO detection. Anti-MHCII signal is gated on the input population. Backgating is shown for $MHCII^{hi}Dex^{lo}$ and $MHCII^{hi}Dex^{hi}$ populations. (bottom) Aggregate enrichment data, n = 3.

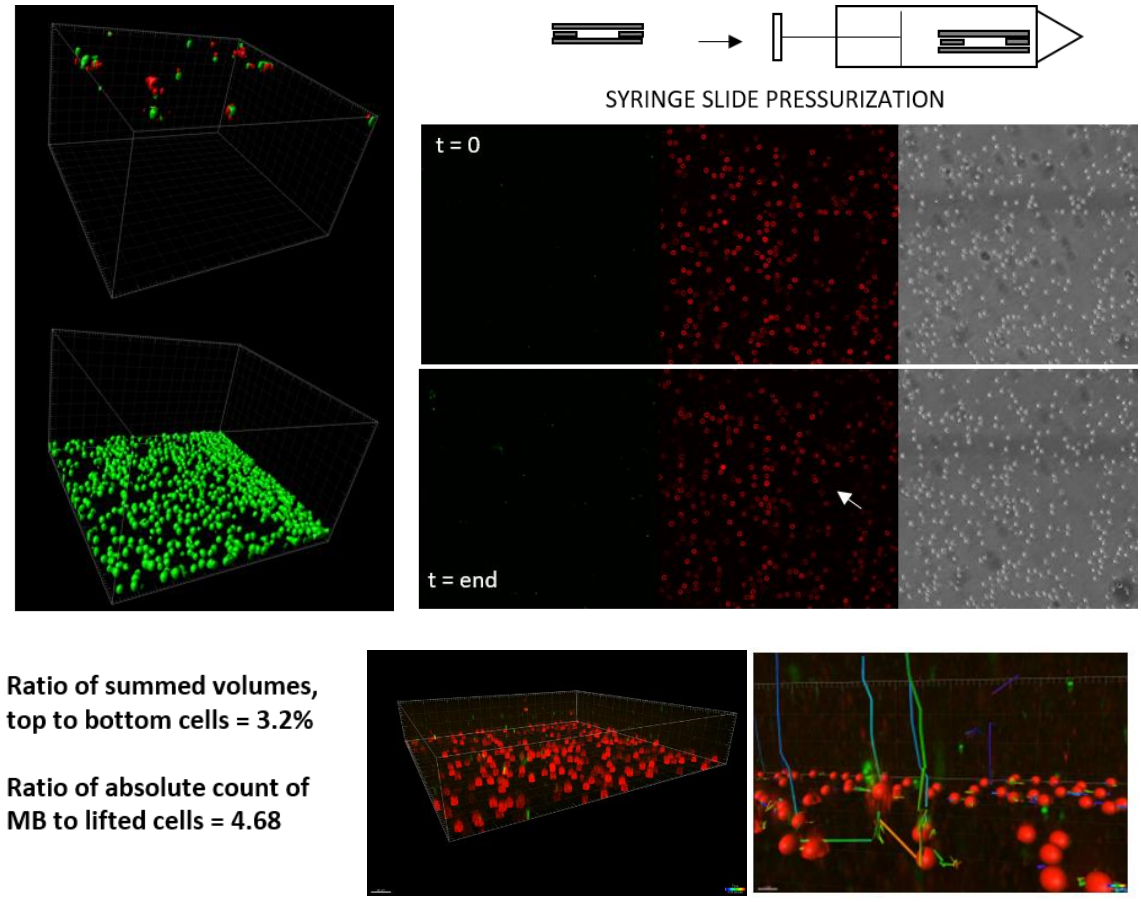

Figure 22. Post-separation crushing visualization. Using the same coverslip sandwich setup as described in Fig 20. Cells are stained with anti-TCRb antibody and the streptavidin-biotinylated P6 MHCII microbubble construct is stained with anti-MHCII antibody. (left) Imaris reconstruction. Isosurface reconstruction of buoyant cells and microbubbles within 10 microns of a cell using the Imaris built-in distance transform function. The ratio of top-to-bottom volumes of cells is 3.2%, which corresponds roughly to the FACS-calculated occurrence of P6 cells. The absolute count of microbubbles to lifted cells is 4.68, which roughly agrees with the theoretical calculation of the microbubble lifting capability. (top right) Microbubble crushing. The coverslip sandwich assembly was placed entirely in a 60 mL syringe, pressurized to 2 atmospheres, and immediately retrieved for imaging. Images are Z-slices over time near the bottom focal plane showing bubble fragments and cells sedimenting. (bottom) Imaris reconstruction of falling cells.

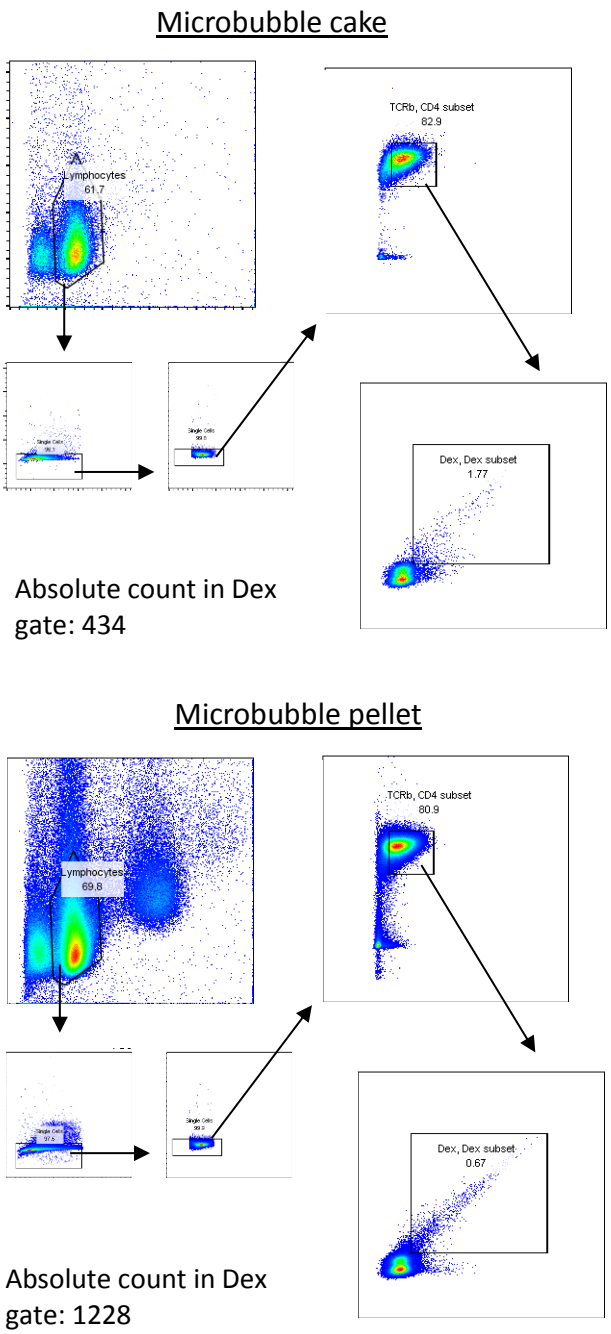

Figure 23. Dextramer-based separation performed as an orthogonal method to confirm separation of P6+ cells using a separate separation construct. Cells are stained with P6 dextramer (APC and PE) after CD4 enrichment. A streptavidin-biotinylated anti-APC microbubble construct is prepared and incubated with dextramer-stained cells, demonstrating that cell enrichment can be achieved after dextramer staining.

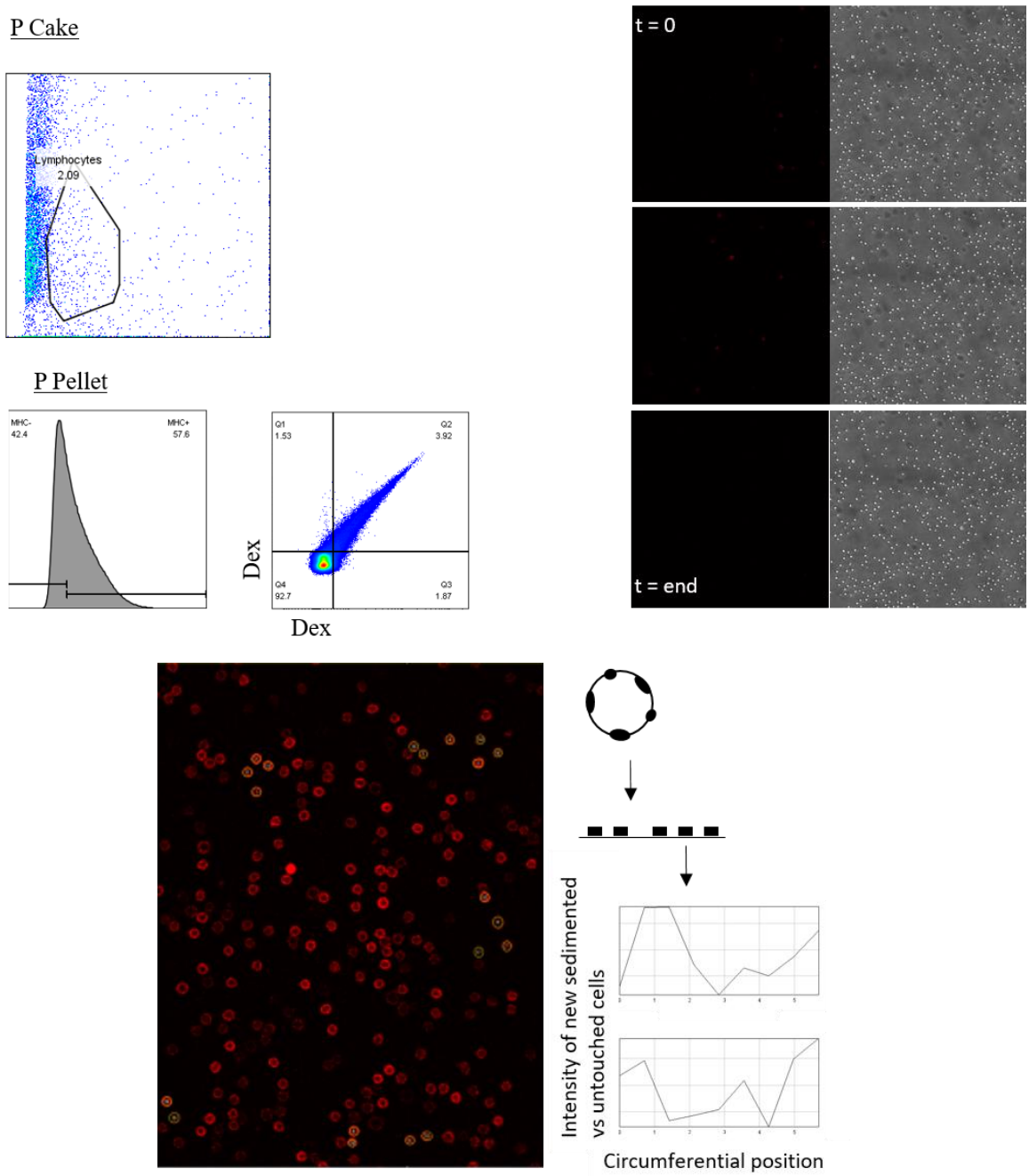

Figure 24. Control bubbles and analysis of sedimented cells. (top left) Control microbubble (perfusion, P, bubble) as negative control, since it lacks any attachment to streptavidin or antibodies. (top right) Microbubble crushing while holding the focal plane at constant distance above sedimented cells to observe cells passing in and out of the focal plane and the corresponding "shadowing" seen on the brightfield signal (bottom) Analysis of TCR clustering of newly sedimented vs. untouched cells using FIJI profile plot function. Example profile plots shown. The difference is not statistically significant between ten selected cells for each category ($p>0.3$ for the two-sample t-test).

Visualization

Owing to the difficulty of seeing cells, I used several computer graphics programs to create visuals. Autodesk Maya is a general purpose animation program. Models were generated either through Maya's built-in modeling functions or repurposed from Autodesk Inventor, a CAD modeling program, or Autodesk Remake, a reconstruction program able to generate 3D models of objects from ordinary photographs.

Animation 1 is a simulation of blood cells in a vessel using Maya's Nucleus dynamics solver. The cells are spheres which collide with each other and the vessel wall. The spheres' geometry has been instanced to a model of an erythrocyte, itself created from simple manipulation of a polygonal cylinder primitive and made more realistic by a one-time random turbulent deformation of a Maya nCloth copy of the surface, which was then converted back into a static polygonal model. Pulsatility in such a vessel facilitated visualization of the cells. This animation is an attempt to balance visual interest with visual fidelity. It is incomplete, but was ultimately meant to show the native environment of an atherosclerotic lesion, including the cellular constituents that would then be collected for analysis.

Animation 2 shows the centrifugation step of the separation protocol. The centrifuge was a 3D reconstruction of the actual lab centrifuge from photographs. The combination adapter is used.

Another visualization was made using the UCSF Chimera program. This program allows for import of Research Collaboratory for Structural Bioinformatics Protein Data Bank (RSCB PDB) crystallography and nuclear magnetic resonance (NMR) data for 3D

visualization. I attempted to even the compromise between representations of the project's facets: cartoons are easy to draw and can be simple to interpret, but appreciation of the complexity and details may be lost. Further, some cartoon scales may be grossly exaggerated. On the other hand, diagrams depicting atomic-scale resolution may be too complex to easily interpret and obscure effective communication. With PDB data, I attempted to avoid rendering too many extraneous details. Some ribbon diagrams are shown to highlight relevant entities and the lipids are fully shown in stylized line art for the outright visual effect, but many other complex structures are hidden and instead represented as surface reconstructions. These are smoothed polygonal models derived from van der Waals radii of constituent atoms. The smoothing is purely subjective and has no justifying basis other than appearance. Transparency, lighting, color, and silhouetting are used to give some models a cel shaded appearance for additional visual effect. 3D labeling is used to give the viewer an additional dimensional cue. Orientation of some molecules, such as TCR, could be inferred, but others are guesses. The model used for TCR, for example, was co-crystallized with the MHCII molecule, so directionality could be determined.

1. Visualization 1 shows the CD4 microbubble construct. A lipid bilayer is shown, representing a target cell and CD3, CD4, and TCR surface proteins. The models are to scale. A lipid monolayer is shown, representing the microbubble. A PEG-2000 (polyethylene glycol with molecular weight 2 kDa) linker connecting the microbubble with a streptavidin molecule is shown, and four immunoglobulin molecules are shown attached. This model raises interesting questions as to the degree of attachment between a microbubble and its target cell, as at first glance it is unclear how many CD4 antibodies

are able to simultaneously attach. Enumerated PDB structures described in Figure 3 were modified and used for this visualization.

2. Visualization 2 shows the TCR-MHCII interaction between an antigen presenting cell and CD4 T cell. Peptide 3K is located in the I-A^b MHCII molecule—it is 13 residues long.

4. Visualization 3 shows the MHCII tetramer reagent.

The Introduction, Results, and Discussion sections do not include published work, work submitted for publication, or material being prepared for publication submission. These sections include results generated as a result of collaboration with Dr. Joshua Rychak (Targeson, La Jolla, CA; University of California San Diego, La Jolla, CA), who provided microbubble reagents, Dr. Marc Jenkins (University of Minnesota, Minneapolis, MN), who provided biotinylated MHCII monomer, and Dr. Zbigniew Mikulski (La Jolla Institute for Allergy and Immunology, La Jolla, CA), who assisted with confocal microscopy. The dissertation author was the principal researcher and author on this dissertation.

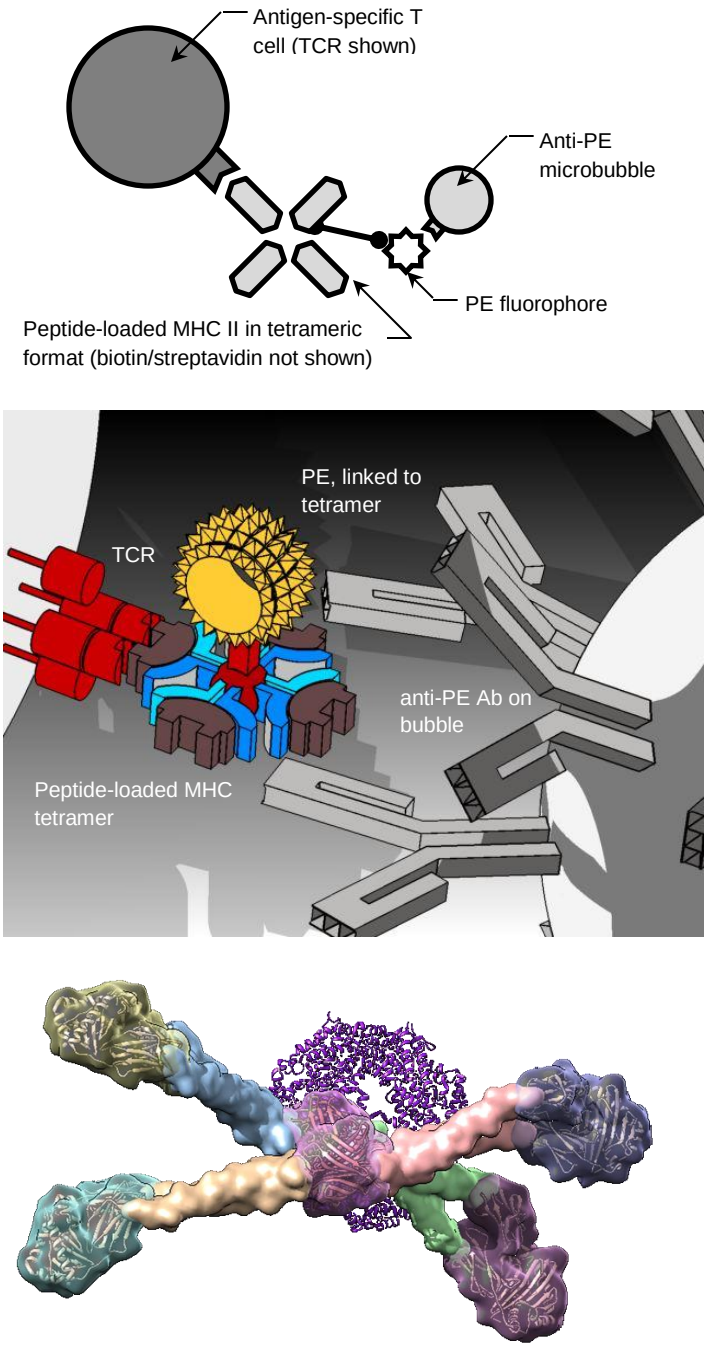

Figure 25. Construct visualization. Three representations of the MHCII tetramer, from cartoon (top) to 3D model (mid) to PDB structural rendering (bottom).

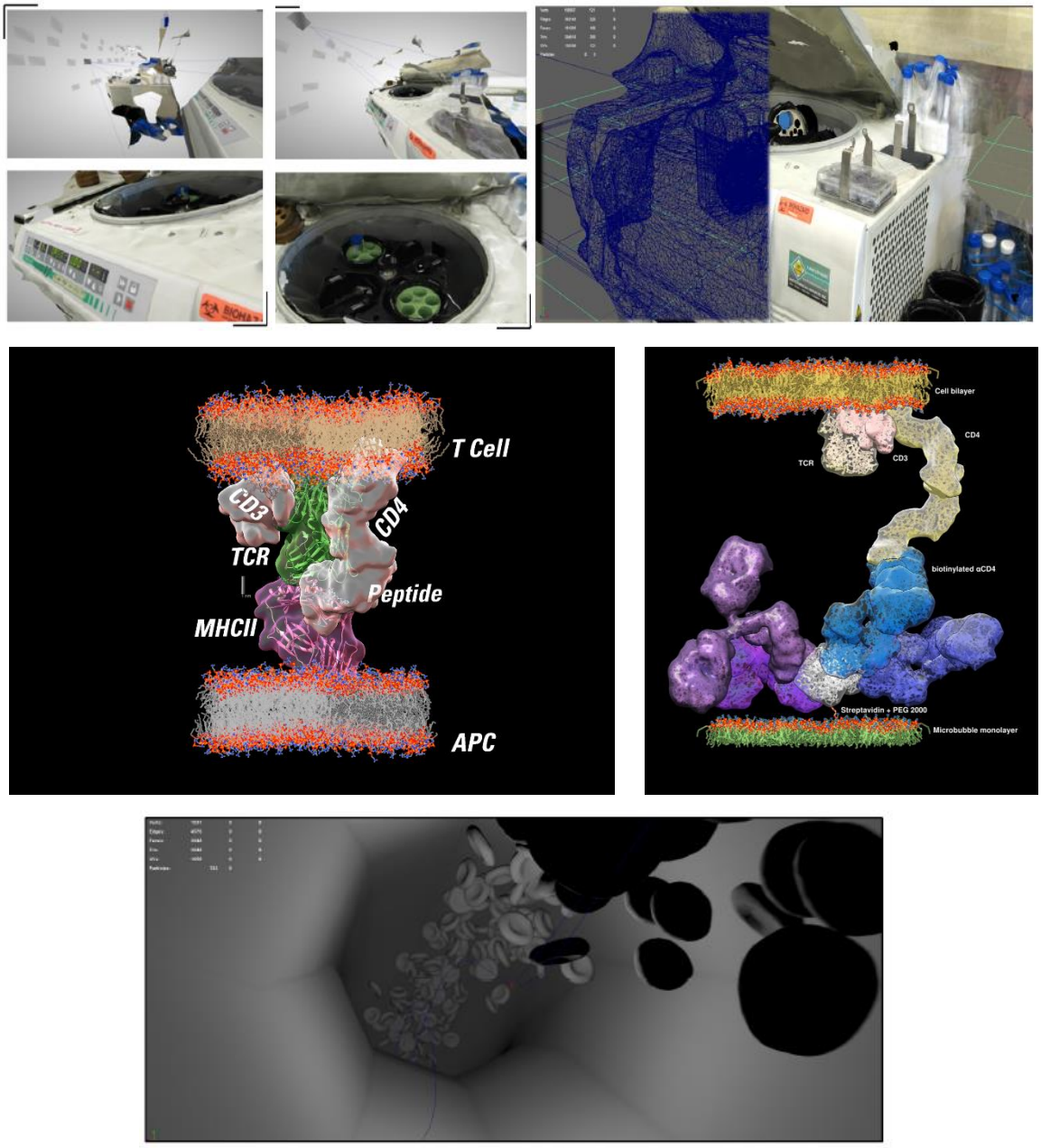

Figure 26. Animation visualization. (top) Centrifugation animation (Animation 2) using a 3D model of the lab centrifuge reconstructed using photogrammetry (reconstruction from photographs). (center left) Model of antigen presentation to a CD4 T cell using PDB structural data. (center right) CD4 microbubble construct using PDB structural data. (bottom) Animation (Animation 1) of red blood cells. These visualizations were originally intended to be combined to show cell separation on several different levels.

DISCUSSION

This project shows the successful separation of antigen-specific T cells using a buoyancy-based method, at the proof-of-concept level, as verified by flow cytometric staining and confocal microscopy. Separation of these cells has not been previously accomplished using this novel separation construct.

B cells and CD4 T cells were bulk-enriched successfully before a method analogous to MHCII multimerization was used to capture antigen-specific cells. MHCII staining indicates that detectable remnants of the separation construct are still attached to the target cells even after crushing, a disappointing find. As conjectured, a plausible failure mode for the persistence of the anti-MHCII signal are the "tetramer-like" entities formed (streptavidin with four attached biotinylated MHCII monomers) during preparation of the separation construct. Since MHCII tetramers have been established to stain cells, they may not readily detach from the cell, even following microbubble implosion.

Important parameters

The separation protocol was not optimized, and the poor separation yields relative to those of commercially available kits for non-rare cell separations indicates room for improvement. There are many factors which may be considered for optimization. For the purposes of this project, the microbubble reagents provided by Targeson were not able to be modified from their collaborator-prepared condition. Future work would be well-

advised to consider the following table of parameters in manufacturing microbubbles for separation as well as for the separation protocol itself.

Some parameters are more influential than others. The parameter space comprises many variables and requires a more careful multiple-parameter sensitivity analysis to better inform future experiments.

Table 4. List of model parameters.

Parameter	**Rationale**
Microbubble dispersion and size	As modeled in Figure 8, small microbubbles have smaller buoyant lifting capacities. In microscopy, some small microbubbles were seen attached to cells on sedimented, bottom focal planes; they were not sufficiently buoyant. Larger microbubbles are more advantageous for separation due to their higher lifting capacity. The ability to produce a homogeneous distribution of microbubble sizes would decrease separation variability.
Microbubble constitution (gas core density, lipid monolayer makeup)	The gas core density affects the buoyancy and thus the lifting capacity of the bubble. The lipid monolayer composition affects the mass of the bubble and thus the buoyancy as well, but also the fluidity (melting temperature) of the microbubble's lipid shell. This in turn affects not only the flexibility of the bubble itself, but also the lateral diffusion of molecular attachments to the bubble, which may impact the microbubble's ability to attach to multiple ligands at once.
Density of surface-attached molecules	Density of molecules such as streptavidin determine the valency of the microbubble—the strength with which the microbubble can attach to a target cell. This may be relevant for separation of rare cell populations with unusually low MHCII-TCR binding affinities, for example.
Size of molecular species attached to microbubble	A spatial consideration prompted by the scaled molecular models I constructed of the separation constructs. There may be steric limitations on the degree of attachment that can be achieved based on the size and positioning of the molecules themselves.
Binding affinity	This parameter is specific to the target cell and the formulation of the microbubble construct, but influences the degree of attachment of the bubble to the target cell.
Incubation time, temperature, mixing volume	Temperature influences membrane fluidity of the target cells and microbubbles, and also the degree of mixing of the two species during the mixing stage of the separation protocol. Mixing volume and time are important to the extent that microbubbles sufficiently encounter cells for attachment.
Microbubble to cell ratio	This parameter likely affects both yield and purity of separations. An insufficient number of microbubbles used to separate cells will suffer from low yield. Conversely, too many microbubbles may buoy contaminating cells nonspecifically into the cake fraction.

Future work and needs

The titrated microbubble separation construct warrants further investigation as a potential workaround to the persistent anti-MHCII signal detectable after implosion of the microbubble fully saturated with P6 MHCII monomer. As shown in Figure 27, an initial attempt at creating such a construct indicated that the titration could be accomplished successfully, but more experimental investigation into employing the construct to do separations is needed.

Further investigation into modeling refinements may be a potential avenue for investigation. The simulations conducted in a previous section to calculate microbubble dynamics are based on simple conditions. Parameters introduced in Table 4 may inform a wide diversity of potential experimental conditions to optimize. As an example, changing the microbubble and cell ratios past a critical threshold causes the assumptions of isolated bubbles and Stokes flow to no longer be valid; aggregates of spherical particles change the drag experienced by each individual particle [41].

In summary, a removable reagent for cell separation of antigen-specific CD4 T cells would be a boon to both clinical and research applications. There is currently no commercial product to fulfill this need. This project describes a proof-of-concept basis for further development of such a product.

The Introduction, Results, and Discussion sections do not include published work, work submitted for publication, or material being prepared for publication submission. These sections include results generated as a result of collaboration with Dr. Joshua

Rychak (Targeson, La Jolla, CA; University of California San Diego, La Jolla, CA), who provided microbubble reagents, Dr. Marc Jenkins (University of Minnesota, Minneapolis, MN), who provided biotinylated MHCII monomer, and Dr. Zbigniew Mikulski (La Jolla Institute for Allergy and Immunology, La Jolla, CA), who assisted with confocal microscopy. The dissertation author was the principal researcher and author on this dissertation.

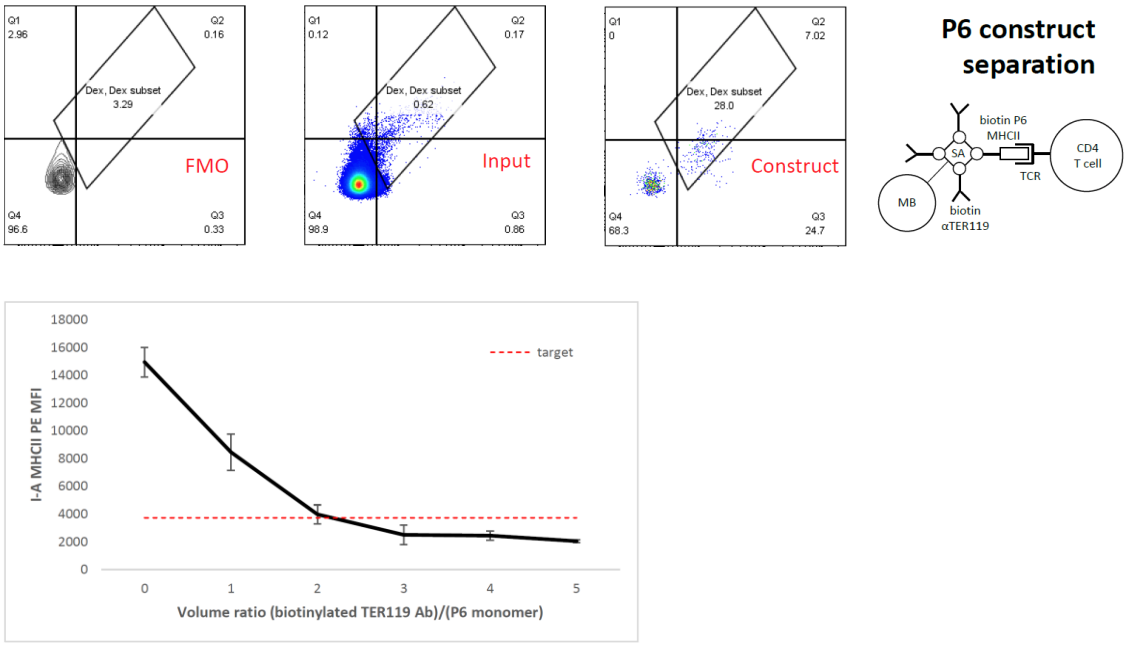

Figure 27. Titrated P6 construct. This was constructed by titrating TER119 antibody against the biotinylated MHCII monomer; ratios of the species were detected by anti-MHCII staining. An initial experiment showed successful separation, but the results could not be repeated.

REFERENCES

[1] Metheny, L., de Lima, M., Gerson, S., Eid, S., & Huang, A. Y. (2014). Intra-Osseous Co-Transplantation of CD34-Selected Umbilical Cord Blood and Mesenchymal Stromal Cells. Blood, 124(21), 3811.

[2] Yun, S. O., Shin, H. Y., Kang, C. Y., & Kang, H. J. (2016). Generation of antigen-specific cytotoxic T lymphocytes with activated B cells. Cytotherapy, in press.

[3] Mitchell, C. J., Getnet, D., Kim, M. S., Manda, S. S., Kumar, P., Huang, T. C., Pinto, S. M., Nirujogi, R. S., Iwasaki, M., Shaw, P. G., Wu, X., Zhong, J., Chaerkady, R., Marimuthu, A., Muthusamy, B., Sahasrabuddhe, N. A., Raju, R., Bowman, C., Danilova, L., Cutler, J., Kelkar, D. S., Drake, C. G., Prasad, T. S., Marchionni, L., Murakami, P. N., Scott, A. F., Shi, L., Thierry-Mieg, J., Thierry-Mieg, D., Irizarry, R., Cope, L., Ishihama, Y., Wang, C., Gowda, H., & Pandey, A. (2015). A multi-omic analysis of human naïve CD4+ T cells. BMC systems biology, 9, 75.

[4] Gordon, S. N., Cecchinato, V., Andresen, V., Heraud, J.-M., Hryniewicz, A., Parks, R. W., … Franchini, G. (2011). Smallpox Vaccine Safety Is Dependent on T Cells and Not B Cells. The Journal of Infectious Diseases, 203(8), 1043–1053.

[5] Flow-cytometric analysis of 11 strains of mice. (2006). Retrieved from http://phenome.jax.org/db/q?rtn=projects/docstatic&doc=Jaxpheno6/Jaxpheno6_Protocol

[6] Moon, J. J., Chu, H. H., Pepper, M., McSorley, S. J., Jameson, S. C., Kedl, R. M., & Jenkins, M. K. (2007). Naïve CD4+ T cell frequency varies for different epitopes and predicts repertoire diversity and response magnitude. Immunity, 27(2), 203–213.

[7] Gorczynski, R. M., Miller, R. G., & Phillips, R. A. (1970). Homogeneity of antibody-producing cells as analysed by their buoyant density in gradients of Ficoll. Immunology, 19(5), 817–829.

[8] Zembala, M., & Asherson, G. L. (1970). The rapid purification of peritoneal exudate macrophages by ficoll (polysucrose) density gradient centrifugation. Immunology, 19(4), 677–681.

[9] Pertoft, H., Rubin, K., KjellÃŠn, L., Laurent, T. C., & Klingeborn, B. (1977). The viability of cells grown or centrifuged in a new density gradient medium, Percoll(TM). Experimental cell research, 2, 449–457.

[10] MACS® MicroBeads. (2016). Retrieved from http://www.miltenyibiotec.com/en/products-and-services/macs-cell-separation/macs-technology/microbeads_dp.aspx

[11] MagniSort™ Frequently Asked Questions. (2016). Retrieved from http://www.ebioscience.com/resources/faq/magnisort-faq.htm

[12] MojoSort™ Magnetic Cell Separation System. (2014). Retrieved from http://www.biolegend.com/mojosort

[13] Dynabeads Products & Technology. (2016). Retrieved from https://www.thermofisher.com/us/en/home/brands/product-brand/dynal/dynabeads-technology.html

[14] Easy 50 EasySep™ Magnet. (2016). Retrieved from https://www.stemcell.com/easy-50-easysep-magnet.html

[15] BD™ IMag Cell Separation System. (2004). Retrieved from https://www.bdj.co.jp/pdf/55-06_04-7900030-2-A1.pdf

[16] Miltenyi, S., Müller, W., Weichel, W., & Radbruch, A. (1990). High gradient magnetic cell separation with MACS. Cytometry, 2, 231–238.

[17] Abts, H., Emmerich, M., Miltenyi, S., Radbruch, A., & Tesch, H. (1989). CD20 positive human B lymphocytes separated with the magnetic cell sorter (MACS) can be induced to proliferation and antibody secretion in vitro. Journal of immunological methods, 1-2, 19–28.

[18] Plouffe, B. D., Murthy, S. K., & Lewis, L. H. (2015). Fundamentals and Application of Magnetic Particles in Cell Isolation and Enrichment. Reports on Progress in Physics. Physical Society (Great Britain), 78(1), 016601.

[19] Shapiro, H. M. (2003). Practical Flow Cytometry, Fourth Edition. Hoboken, New Jersey: John Wiley & Sons, Inc.

[20] Hu, W., Berdugo, C., & Chalmers, J. J. (2011). The potential of hydrodynamic damage to animal cells of industrial relevance: current understanding. Cytotechnology, 63(5), 445–460.

[21] Mollet, M., Godoy-Silva, R., Berdugo, C., & Chalmers, J. J. (2008). Computer simulations of the energy dissipation rate in a fluorescence-activated cell sorter: Implications to cells. Biotechnology and bioengineering, 2, 260–272.

[22] Cotter, M. J., Norman, K. E., Hellewell, P. G., & Ridger, V. C. (2001). A Novel Method for Isolation of Neutrophils from Murine Blood Using Negative

Immunomagnetic Separation. The American Journal of Pathology, 159(2), 473–481.

[23] Unnikrishnan, S., & Klibanov, A. L. (2012). Microbubbles as ultrasound contrast agents for molecular imaging: preparation and application. AJR. American journal of roentgenology, 2, 292–299.

[24] Rychak, J. J., Lindner, J. R., Ley, K., & Klibanov, A. L. (2006). Deformable gas-filled microbubbles targeted to P-selectin. Journal of controlled release: official journal of the Controlled Release Society, 3, 288–299.

[25] Dayton, P. A., & Rychak, J. J. (2007). Molecular ultrasound imaging using microbubble contrast agents. Frontiers in bioscience: a journal and virtual library, 5124–5142.

[26] Green, N. M. (1966). Thermodynamics of the binding of biotin and some analogues by avidin. Biochemical Journal, 101(3), 774–780.

[27] Jenkins Lab MHC Class II Tetramer Production Protocol – 01/08/16. (2016). Retrieved from http://www.jenkinslab.umn.edu/Jenkins_Lab_2/assets/pdf/New%20tetramer%20production%20010816-TD.pdf

[28] Subbramanian, R. A., Moriya, C., Martin, K. L., Peyerl, F. W., Hasegawa, A., Naoi, A., Chhay, H., Autissier, P., Gorgone, D. A., Lifton, M. A., Kuus-Reichel, K., Schmitz, J. E., Letvin, N. L., & Kuroda, M. J. (2004). Engineered T-cell receptor tetramers bind MHC-peptide complexes with high affinity. Nature biotechnology, 11, 1429–1434.

[29] Tse, K., Gonen, A., Sidney, J., Ouyang, H., Witztum, J. L., Sette, A., Tse, H., & Ley, K. (2013). Atheroprotective Vaccination with MHC-II Restricted Peptides from ApoB-100. Frontiers in immunology, 4, 493.

[30] Li, J., Zhao, X., Skoff, R., Shaw, M. K., & Tse, H. Y. (2011). DIFFERENTIAL LEVELS OF RESISTANCE TO DISEASE INDUCTION AND DEVELOPMENT OF RELAPSING EXPERIMENTAL AUTOIMMUNE ENCELPHALOMYELITIS IN TWO H-2b-RESTRICTED MOUSE STRAINS. Journal of Neuroimmunology, 234(1-2), 109–114.

[31] Li, J., Ridgway, W., Fathman, C. G., Tse, H. Y., & Shaw, M. K. (2007). High Cell Surface Expression of CD4 Allows Distinction of CD4+CD25+ Antigen-specific Effector T Cells from CD4+CD25+ Regulatory T Cells in Murine Experimental Autoimmune Encephalomyelitis. Journal of Neuroimmunology, 192(1-2), 57–67.

[32] Kadowaki, A., Miyake, S., Saga, R., Chiba, A., Mochizuki, H., & Yamamura, T. (2016). Gut environment-induced intraepithelial autoreactive CD4+ T cells suppress central nervous system autoimmunity via LAG-3. Nature Communications, 7, 11639.

[33] Standard Test Method for Automated Analyses of Cells—the Electrical Sensing Zone Method of Enumerating and Sizing Single Cell Suspensions. (2016). Retrieved from https://www.astm.org/Standards/F2149.htm

[34] Vi-CELL XR. (2016). Retrieved from http://www.beckman.com/particle/instruments/cell-sizing-and-processing/vi-cell-xr

[35] Hemavet 950 New, Fast, Veterinary Multi-species Hematology System. Retrieved from http://www.drew-scientific.com/index.html?content=http%3A//www.drew-scientific.com/products/hvconsumables.htm

[36] Williams, J. L., Kithcart, A. P., Smith, K. M., Shawler, T., Cox, G. M., & Whitacre, C. C. (2011). Memory cells specific for myelin oligodendrocyte glycoprotein (MOG) transfer experimental autoimmune encephalomyelitis. Journal of Neuroimmunology, 234(0), 84–92.

[37] Schmoeckel, K., Traffehn, S., Eger, C., Pötschke, C., & Bröker, B. M. (2015). Full Activation of CD4+ T Cells Early During Sepsis Requires Specific Antigen. Shock (Augusta, Ga.), 43(2), 192–200.

[38] Targeson SOP for microbubble-based cell separation. Provided by Targeson, Inc.

[39] Jones, F. D., Ryffel, H. H., & McCauley, C. J. (2000). Machinery's Handbook Guide 26. New York: Industrial Press.

[40] Kim, N-H. & Sankar, B. V. (2009). Introduction to Finite Element Analysis and Design. Wiley.

[41] Chapman, G. B., & Cokelet, G. R. (1998). Flow resistance and drag forces due to multiple adherent leukocytes in postcapillary vessels. Biophysical journal, 6, 3292–3301.

Citations for UCSF Chimera and associated PDB models are provided inline with Figure 3.